

Galactic environment and the 10- μ m silicate feature of young stellar objects

J. E. Bowey,^{1,2*} A. J. Adamson³ and J. A. Yates¹

¹*Department of Physics and Astronomy, University College London, Gower Street, London WC1E 6BT*

²*Department of Physics, Queen Mary, University of London, Mile End Road, London E1 4NS*

³*UK Infrared Telescope (UKIRT), Joint Astronomy Centre, 660 N. A'ohōkū Place, Hilo, HI 96720, USA*

Accepted 2002 December 16. Received 2002 December 12; in original form 2002 August 16

ABSTRACT

Disc and sphere dust models are used to fit 8–13 μ m flux spectra of 19 low-mass young stellar objects (YSOs) and five Herbig AeBe stars. The 13 non-photospheric low-mass YSOs in quiescent environments and the five Herbig AeBe stars have mean disc temperature indices of 0.4, indicating that the emission arises from optically thin layers above a flared optically thick disc; 10 out of 14 of the low-mass YSO and four out of five of the Herbig AeBe features contain an optically thin silicate emission component. The radius of the peak 10- μ m emission for nine out of the 13 low-mass YSOs is 10–130 au, and three out of the five Herbig AeBe stars are 10–30 au in size. In contrast, the five YSOs from disrupted molecular clouds that have been shaped by expanding supernova remnants have temperature indices of between 0.3 and 0.8; four out of the five are optically thick and three out of the five have radii $\lesssim 2$ au. The photosphere-like continuum of Taurus-Elias 18 could be fitted only with truncated optically thick models, implying the presence of a void between the >500 K and cold ($\lesssim 100$ K) foreground dust. Silicates surrounding low-mass YSOs in quiescent molecular clouds are similar to those in the Trapezium region of the Orion Nebula except when $A_V \lesssim 2$ mag. In the low- A_V case and in low-mass YSOs in disrupted molecular clouds the silicates are similar to circumstellar dust around the evolved star μ Cephei.

Key words: circumstellar matter – infrared: stars.

1 INTRODUCTION

The 10- μ m spectra of young stellar objects (YSOs) and Herbig AeBe stars provide an opportunity to study the physical properties of these systems and the mineralogy of silicate dust. The spectrum observed depends on the radial temperature distribution of dust within the protostar, the density of material in its local environment and the orientation of the YSO with respect to the observer and the chemistry and density of cold foreground material. Hence, the silicate spectra of these objects vary widely and are characterized by emission from dust with a range of temperatures and optical thicknesses, and differing degrees of absorption from cold foreground silicates. Bowey & Adamson (2001, hereinafter Paper I) modelled the non-photospheric 10- μ m continua of T Tauri stars HL Tau and Taurus-Elias 7, which have strong silicate absorption features, with 1000–70 K emission from a one-dimensional disc model with radial power-law temperature and mass–density distributions.

In a flat optically thick disc the radial temperature distribution is $T \propto r^{-0.75}$ (e.g. Adams, Lada & Shu 1988). However, in Paper I we

obtained temperature indices of 0.44 and 0.33 for HL Tau and Elias 7, respectively, and a significant component of optically thin emission in HL Tau. There are two possible sources of the difference between the theory and our results: (i) the mid-plane radial temperature index in the 200–300 K temperature range can be reduced by the effects of grain condensation and evaporation on opacity (Boss & Yorke 1996), (ii) the infrared (IR) emission is from a flared disc with optically thin outer layers as in the Chiang & Goldreich (1997) model; in this model the respective temperature distributions of the inner, optically thick, and the outer, optically thin, regions are $T_{\text{inner}} \propto r^{-1/2}$ and $T_{\text{surface}} \propto r^{-0.4}$.

Here we use simple disc and sphere models with radial temperature and density distributions to model previously published 10- μ m spectra of low-mass YSOs and Herbig AeBe stars.

2 THE SAMPLED OBJECTS

The 10- μ m spectra modelled in this paper (see Fig. 1) are of five T Tauri stars (Hanner, Brooke & Tokunaga 1995, hereinafter HBT1995) in the ρ Oph molecular cloud; seven T Tauris in the Taurus molecular cloud complex (Bowey, Adamson & Whittet 1998; Hanner, Brooke & Tokunaga 1998, hereinafter HBT1998).

*E-mail: jeb@star.ucl.ac.uk

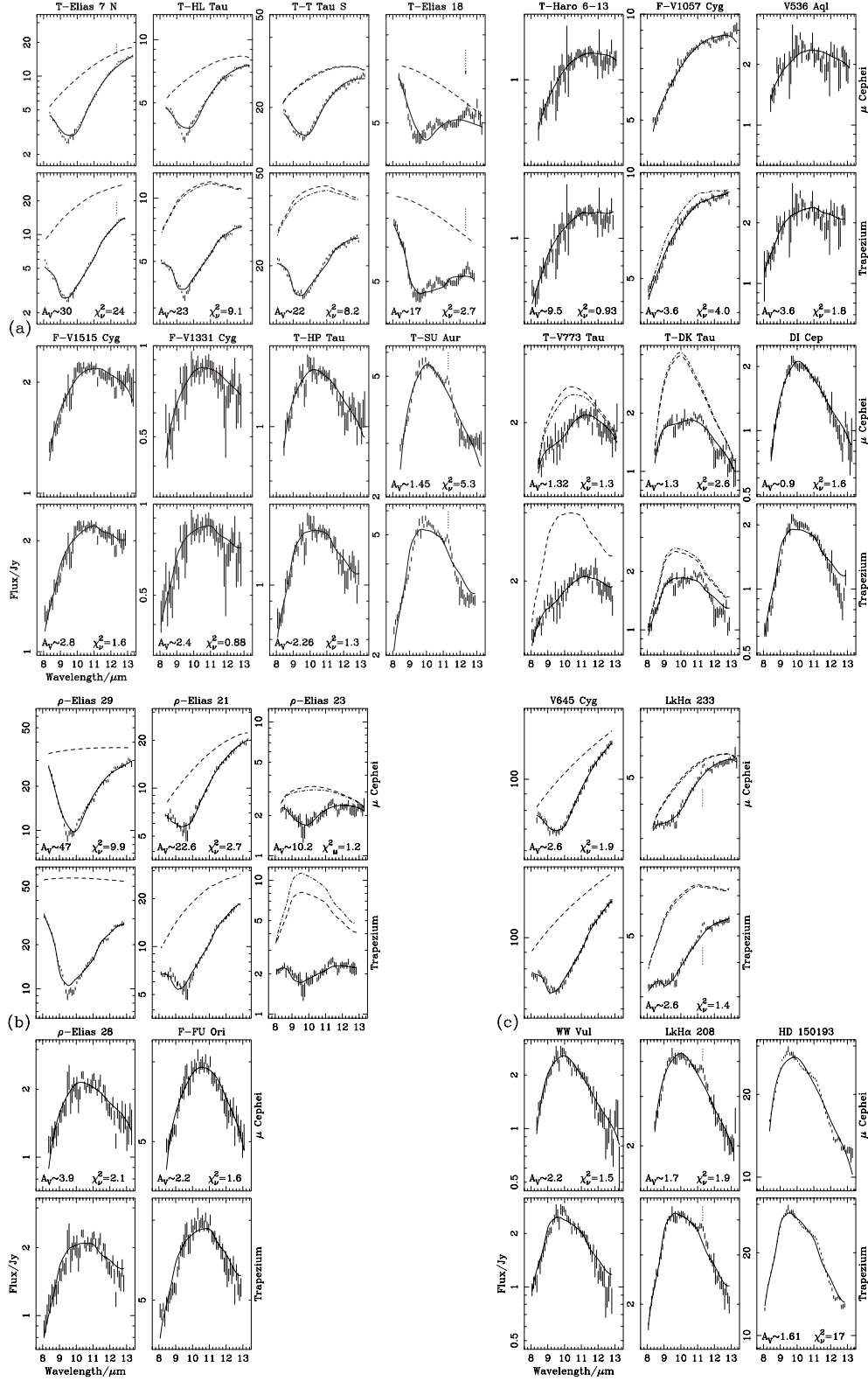


Figure 1. Disc and spherical model fits (solid lines) to the 10- μ m spectra of T Tauri- and FU Ori-type stars in (a) quiescent and (b) disrupted environments and (c) to Herbig AeBe Stars. Continua obtained with the disc model are dashed, if continua obtained with the spherical model differ these are denoted with dot-dashed lines. Fits with the preferred silicate emissivity are labelled with the visual extinction of the source and χ^2_v of the disc model fit. Vertical dotted lines indicate the positions of the 11.3- μ m PAH and 12.3- μ m 7-6 hydrogen lines, which were excluded during fitting.

Table 1. 10- μm spectra of T Tauri, FU Ori and Herbig AeBe stars with published spectral types (SpT) and visual extinction estimates.

Source ^a	Ref ^b	SpT	A_V /mag	Range ^c	Section
Low-mass YSOs					
Quiescent environments					
T-HL Tau	1	K7V	23	NIR	Paper I
T-Elias 18	2	B5	17	NIR	4.9
T-Elias 7 N	1	K5V	6–10	NIR	A1.1
			30	10 μm	4.8
T-T Tauri S	3	K7	5–10	NIR	A1.2
			22	10 μm	4.8
T-Haro 6-13	3	?	9.5	NIR	A1.3
F-V1057 Cyg	3	K1V	3.6	V	A2.1
V536 Aql	3	K7	3.6	V	A2.2
F-V1515 Cyg	3	K2	2.8	V	A2.3
F-V1331 Cyg	3	G-F	2.4	V	A2.4
T-HP Tau	3	K3	2.26	V	A1.4
T-SU Aur	3	G2III	1.45	V–NIR	A1.5
T-V773 Tau	3	K3	1.32	V	A1.6
T-DK Tau	3	K9+M1	1.3	V	A1.7
DI Cep	3	G8IV	0.9	V	A2.5
Disrupted environments					
ρ -Elias 29	5	?	47	NIR	B1.1
ρ -Elias 21	5	M2	22.6	NIR	B1.2
ρ -Elias 23	5	K5–M2	10.2	NIR	B1.3
ρ -Elias 28	5	G5–K7	3.9	NIR	B1.4
F-FU Ori	3	G0I	2.2	V	B2
Herbig AeBe stars					
V645 Cyg	3	A0I	2.6	V	C0.1
LkH α 233	3	A7	2.6	V	C0.2
LkH α 208	3	B7	1.7	V	C0.3
HD 150193	4	A2	1.61	V	C0.4
WW Vul	3	A0–A3	0.64	V	C0.5

^aT indicates that the source is a T Tauri star embedded in the Taurus molecular cloud; F indicates that the star is of FU Ori type; ρ indicates the source is a T Tauri star embedded in the ρ -Oph molecular cloud; V536 Aql and DI Cep are isolated T Tauri stars and the other sources are Herbig AeBe stars.

^bReferences for modelled 10- μm spectra: 1 = Paper I, 2 = Bowey et al. (1998), 3 = HBT1998, 4 = Sylvester & Mannings (2000), 5 = HBT1995.

^cWavelength range for determination of A_V : V, optical B to R bands; NIR, J , H and/or K bands; 10 μm , comparison between TMC YSO silicate absorption features.

Spectra of two other isolated T Tauri, four (low-mass) FU Ori stars and four other Herbig AeBe stars were also taken from HBT1998. The spectrum of the Herbig AeBe star HD150193 is taken from Sylvester & Mannings (2000). The sources, adopted spectral types and A_V s are given in Table 1; the published properties of the sources are discussed in the appendices listed in column 6.

HBT1995 and HBT1998 attempted to reproduce the observed spectrum with four simple models that did not consider the geometry of the source: case (i) allowed for variable optical depth in the circumstellar emission; case (ii) allowed for single-temperature optically thick emission and single-temperature optically thin emission from silicates, whilst cases (iii) and (iv), respectively, modelled optically thin emission with foreground absorption and optically thick emission with foreground absorption. In all of these cases wavelength power laws were invoked to represent the single-temperature emission components. A power law is an appropriate representation of the Rayleigh–Jeans photospheric flux at 10 μm . However, we find that optically thin 10- μm emission from silicates is frequently dominated by grains with a relatively small range of temperatures \sim 100–300 K for which the blackbody emission peaks nearer (or

within) the 10- μm band so that the spectrum in the region of the silicate feature cannot be approximated by a single power law. In addition, none of these models allowed for the presence of optically thick emission, optically thin emission and foreground absorption in a single sightline. The results included herein indicate that several of these spectra contain all three components. We also revise our own models for Elias 7 from paper I and for Elias 18 from Bowey et al. (1998) and, for completeness, include the spectrum of HL Tau modelled in Paper I.

Details of the observations and reduction to flux spectra are given in the original publications; the data were generally selected on the basis of the signal-to-noise (S/N) ratio of the 10- μm spectra. Recently published *ISO* PHOT-S spectra of Cha I T Tauris and SWS spectra of Herbig AeBe stars published by Natta, Meyer & Beckwith (2000) and Meeus et al. (2001), respectively, were not included because of their relatively low quality, and the limited wavelength coverage of the silicate feature in the PHOT-S data (5.9–11.7 μm). An excellent spectrum of the Herbig AeBe star LkH α 198 from HBT1998 was excluded because the unresolved binary components (separated by \sim 5.5 arcsec) have similar MIR fluxes and N -band images suggest the primary has a silicate emission feature, whilst the secondary has deep silicate absorption (Lagage et al. 1993). Hereinafter T indicates that the source is a T Tauri star embedded in the Taurus molecular cloud; F indicates that the star is of FU Ori type; ρ indicates that the source is a T Tauri star embedded in the ρ -Oph molecular cloud; all other sources are Herbig AeBe stars.

3 THE SAMPLED ENVIRONMENTS

The ρ Ophiuchus molecular cloud (ρ MC) and the environment of FU Ori have been shaped by expanding shells caused by supernova explosions in neighbouring OB associations. Therefore, we call low-mass YSOs in these environments ‘disrupted-region’ YSOs and the other low-mass sources ‘quiescent-region’ YSOs.

3.1 Quiescent environments

3.1.1 The Taurus molecular cloud (TMC)

At only 140 pc, the Taurus molecular cloud complex is one of the closest star formation regions. In CO maps its filamentary clouds cover an angular area \sim 230 deg² with a modest CO mass of \sim 3.5 \times 10⁴ M_{\odot} (Ungerechts & Thaddeus 1987). Structures within the cloud have a characteristic size scale of 0.25–0.5 pc (Blitz & Williams 1997). Deep 3.1- μm H₂O ice absorption features (e.g. Smith, Sellgren & Tokunaga 1989; Smith, Sellgren & Brooke 1993; Whittet et al. 1988; Murakawa, Tamura & Nagata 2000) and 4.67- μm CO ice absorption features (Chiar et al. 1995; Teixeira, Emerson & Palumbo 1998) towards the field stars and YSOs at A_V s above only 2–5 mag are indicative of the low interstellar radiation field, clumpy and quiescent nature of the cloud. This change in dust properties is borne out by observations of the 0.35–2.2 μm interstellar linear polarization (see e.g. Whittet et al. 2001): for $0 < A_V < 3$ the extinction and alignment of the grains is similar to that in the diffuse interstellar medium (ISM) ($R_V \sim 3.0$). However, at higher A_V values the extinction increases to the molecular cloud values ($R_V \sim 3.5$ –4.5).

YSOs in this sample are confined mainly to regions near Heiles Cloud 2 in the centre of the complex: Elias 18 (Lynds 1538), DK Tau (L1521), V773 Tau (L1495), Elias 7 and Haro 6–13 (L1528), HP Tau (L1536). HL Tau (L 1551) and T Tau (L1546) are located SE of the centre and SU Aur is NE of the centre in L1505.

The spectra and fits of the sampled T Tauri stars are plotted in Fig. 1(a). Generally as the degree of visual obscuration decreases the 10- μm profile changes from a strong silicate absorption feature with a rising continuum (HL Tau, Elias 7 and T Tau; the photosphere-like continuum of Elias 18 will be discussed in Section 4.9), to a rising, largely structureless emission feature (Har06-13, V1057 Cyg, V536 Aql, V1515 Cyg, V1331 Cyg), to one of strong silicate emission (HP Tau, SU Aur, DI Cep). The possible exceptions to this rule are the relatively noisy spectra of V773 Tau and DK Tau. Since results for the isolated T Tauris DI Cep and V536 Aql were similar to those for the TMC sources the spectra and results for these objects are grouped together.

3.2 Disrupted environments

3.2.1 The ρ Oph molecular cloud (ρMC)

The dark molecular clouds in the Ophiuchus region are in front of the Scorpio-Centaurus OB association, the closest association of early-type stars to the Sun. The youngest of the OB associations is the expanding (-12 km s^{-1}) H I shell produced by a supernova explosion in the background Upper Scorpius association 1.5 Myr ago (de Geus 1992). The T Tauris Elias 21, 23, 28 and 29 are embedded in the foreground ρ Oph molecular cloud (L1688), which is the densest region of an elongated SE–NW-orientated filament that extends from $(l, b) = (3^\circ, 5^\circ)$ to $(353^\circ, 16^\circ)$ (complex 3; de Geus, Bronfman & Thaddeus 1990). de Geus (1992) showed that the ρ Oph molecular cloud (ρMC) is the remnant of a larger, slower-moving (3 km s^{-1}) complex that was fragmented by shocks associated with the passing Upper Scorpius H I shell. In contrast with the virtually scale-free $r \sim 30\,000 \text{ au}$ isolated protostellar envelopes observed in the TMC, 1.3-mm continuum maps of L1688 show that embedded Class I and Class 0 YSOs merge with surrounding emission at a finite radius of only $\lesssim 5000 \text{ au}$ (Motte, Andre & Neri 1998). The 10- μm spectra of the ρ Oph YSOs (Fig. 1b) include a very wide range in visual extinction (3.9–47 mag) and changes in the spectra with visual extinction are similar to those for TMC sources.

3.2.2 FU Ori

FU Ori (Fig. 1b) is the prototype of a class of young stellar objects that have undergone photometric outbursts on the order of 4–6 mag in less than 1 yr (Herbig 1966). The system lies behind the head of B35, a bright-rimmed cometary globule and site of low- to intermediate-mass star formation, on the NW rim of the λ Orionis CO ring surrounding an OB association (Lang et al. 2000).

3.3 Herbig AeBe stars

The sampled Herbig AeBe stars are widely spaced in the galactic plane, the spectra, fits and estimated continua are shown in Fig. 1(c). V645 Cyg is the most distant of the observed sources at 3.5 kpc; LkH α 233 is below the galactic plane in condensation A of the Lac OB1 molecular cloud; WW Vul is isolated and is obscured by clouds in the Vul Rift; LkH α 208 is in front of the Gem OB1 molecular cloud complex; and HD 150193 is in a 5 km s^{-1} filament in complex 3 of the Ophiuchus molecular cloud, to the SE of the ρ Oph molecular cloud.

In comparison with the T Tauri stars the measured optical extinction towards these sources is low ($A_V \sim 1.6\text{--}2.6 \text{ mag}$). However, the difference in their silicate features is as extreme as for the T Tauris.

The spectra of V645 Cyg and LkH α 233 display silicate absorption features, whilst those of WW Vul, LkH α 208 and HD 150193 are indicative of optically thin silicate emission.

4 MODELS

4.1 Temperature and mass density distributions

Following the method of Paper I we assume that emission from the young stellar object is modified by dust grains, the temperature of which is a function of radial distance from the photosphere, i.e.

$$T(r) = T_* \left(\frac{R_*}{r} \right)^q, \quad (1)$$

where T_* is the temperature at the stellar radius R_* and q is the temperature index of the modified stellar radiation field produced by the dust grains in the circumstellar environment; a subscript d denotes the disc model and a subscript s denotes the spherical model.

In the disc the mass density distribution is a function of its surface area,

$$\Sigma(r) = \Sigma_* \left(\frac{R_*}{r} \right)^{p_d}, \quad (2)$$

where Σ_* is the area mass density at R_* and p_d is the disc density index. However, in the spherical model ρ_* is the volume mass density at R_* so that equation (2) becomes

$$\rho(r) = \rho_* \left(\frac{R_*}{r} \right)^{p_s} \quad (3)$$

and p_s is the radial volume density index.

4.2 Emission from discs and spheres

The equation for the disc flux obtained in Paper I is

$$F_{\text{disc}} = a \int_{T_D}^{T_0} B_\nu(T) [1 - e^{-c\epsilon_\nu r(T)^{-p_d}}] r(T)^{q_d+2} dT, \quad (4)$$

where $r(T)$ is obtained from equation (1), and T_0 and T_D are, respectively, the temperatures of the inner and outer edges of the region of the disc that emits in the 10- μm band, θ is the angle of inclination of the disc to the sky plane. The optical depth of the silicate emission, $\tau_d(r, \theta)$ is given by the exponent $c\epsilon_\nu r(T)^{-p_d}$, where ϵ_ν is the normalized 10- μm silicate emissivity (i.e. the shape of the 10- μm silicate absorption/emission feature normalized to unity at the wavelength of its peak) and $p_d = 7/4$; the scale of the exponent, c is given by

$$c = \frac{k \Sigma_0 R_0^{p_d}}{\cos \theta}, \quad (5)$$

where k is the mass absorption coefficient when $\epsilon_\nu = 1$ and Σ_0 and R_0 are defined as the surface mass density and radius at the inner edge of the *silicate* disc where $T(r) = T_0$. R_0 is estimated from equation (1), with $R_* = 2 R_\odot$, the radius of a typical T Tauri star. The scale of the disc flux, a , is given by

$$a = \frac{2\pi \cos \theta}{D^2 q_d T_0 R_0^{q_d}}. \quad (6)$$

The observed flux density of a sphere at distance, D , is equal to the product of the flux emitted by the source and its surface area divided by the distance to the source.

$$F_{\text{vsphere}} = \frac{1}{4\pi D^2} \int_{R_*}^{R_S} B_\nu[T(r)] [1 - e^{-\tau_\nu(r)}] 4\pi r^2 dr. \quad (7)$$

Since the orientation of the sphere to the sky plane does not affect the projected area, there is no angular dependence. Following Paper I and integrating over temperature instead of radius, this becomes

$$F_{\text{vsphere}} = b \int_{T_S}^{T_0} B_{\nu}(T) [1 - e^{-s\epsilon_{\nu}r(T)^{-p_s}}] r(T)^{q_s+3} dT, \quad (8)$$

where $r(T)$ is obtained from equation (1), and T_0 and T_S are, respectively, the temperatures of the inner and outer edges of the region of the sphere that emits in the 10- μm band. The scale of F_{vsphere} , b , is given by

$$b = \frac{1}{D^2 q_s T_0 R_0^{q_s}}. \quad (9)$$

In the optically thin case the emission optical depth is given by

$$\tau_{\nu}(r) = K_{\nu} \rho(r) = k' \epsilon_{\nu} \rho(r), \quad (10)$$

where K_{ν} is the bulk absorption coefficient of material in the sphere and k' is the scale of the silicate emissivity. The optical depth of the emission becomes

$$\begin{aligned} \tau_{\nu}(r) &= k' \epsilon_{\nu} \rho \left(\frac{R_0}{r} \right)^{p_s} \\ &= s \epsilon_{\nu} r(T)^{-p_s}, \end{aligned} \quad (11)$$

where

$$s = k' \rho_0 R_0^{p_s} \quad (12)$$

and ρ_0 and R_0 are defined as the volume mass density and radius at the inner edge of the *silicate* sphere where $T(r) = T_0$. The most probable density distribution would come about via infall ($p_s = 3/2$) or outflow ($p_s = 2$; Beckwith et al. 1990).

In the optically thick case [i.e. when $\tau_{\nu d}(r, \theta)$, $\tau_{\nu s}(r) \rightarrow \infty$] the integrands of equations (4) and (8) differ only in the indices of the radial temperature distribution; substituting for $r(T)$ from equation (1) it is found that $q_s \approx 3/2 q_d$. Similarly, in the very optically thin case [when $\tau_{\nu d}(r, \theta)$, $\tau_{\nu s}(r) \rightarrow 0$] the exponents become important, so that $q_s \approx 4 q_d$.

4.3 Foreground extinction

The intrinsic flux of the disc or sphere is extinguished by material in its cooler outer regions and the foreground molecular cloud. In the 10- μm band the resulting extinction is characterized by a power-law continuum extinction modified by an absorption feature owing to the Si–O stretch in silicates.¹ Hence, the flux *observed*, F_{ν} , is given by

$$F_{\nu} = F_{\text{vemiss}} e^{-\tau_{\text{cont}}(\lambda)} e^{-c_{\text{sil}} \epsilon_{\nu}}, \quad (13)$$

where F_{vemiss} is given by F_{vdisc} or F_{vsphere} as appropriate. c_{sil} is the optical depth of the foreground silicate absorption feature modelled with the silicate emissivity, ϵ_{ν} (we use the standard assumption that the optical properties of the heated and cold silicates are the same). $\tau_{\text{cont}}(\lambda)$, is the continuum extinction optical depth that is assumed (as in Paper I) to vary as a power law longwards of the H band.

$$\tau_{\text{cont}}(\lambda) = \tau_{\text{cont}}(1.65 \mu\text{m}) \left(\frac{\lambda}{1.65} \right)^{-1.8}, \quad (14)$$

¹ These terms are separate because the dust is composed of other materials as well as silicates and by silicates with a wide variety of grain sizes, which will not all contribute to the 10- μm feature.

the exponent (-1.8) is the mean value obtained by Martin & Whittet (1990). H -band extinctions were derived from estimates of A_{ν} , using the extinction law for the ρ Oph molecular cloud (Whittet 1992) since none is determined for the TMC.

4.4 Modelling emissivities, ϵ_{ν}

The silicate emissivities used for modelling the observed spectra are those that were found to be most similar to the absorption spectra of other modelled astronomical sources (see Paper I and Bowey et al. 1998). In our experience no laboratory spectrum of a single amorphous silicate has produced a good match to the astronomical data (see Bowey & Adamson 2002); therefore we use only astronomical emissivities: of dust in the Trapezium region of the Orion Nebula (Forrest, Gillett & Stein 1975) and the circumstellar O-rich dust around μ Cephei (Russell, Soifer & Forrest 1975). Both emissivities are derived by dividing the observed spectrum by a 250-K blackbody (see Section 6.1 for further discussion).

4.5 Fitting procedure

The 10- μm spectra were fitted with the disc and sphere models. As in Paper I, the radial density indices were fixed to values indicated by theory, namely $p_d = 7/4$ for discs and $p_s = 2$ for spheres and parameters were initialized with optically thin silicate emission and foreground silicate absorption.

Up to four parameters were fitted by means of χ^2_{ν} minimization. For the disc and sphere models the fitted parameters were (respectively) the flux scale (a or b), temperature index (q_d or q_s), the scale of the silicate emission feature (c or s) and the scale of the foreground silicate absorption feature (c_{sil}). However, preliminary fits to some of the observed spectra indicated that (i) the optical depth of the silicate emission was unconstrained and/or (ii) that the foreground absorption, was close to zero. In case (i) the scale of the silicate emission parameters were fixed to force the emission to be optically thick and in case (ii) c_{sil} was set equal to zero to produce stable fits.

The fixed parameters, the modelling silicate emissivities and resulting temperature indices, silicate absorption optical depths and χ^2_{ν} of the fits are listed in Table 2; preferred fits are typed in bold. We prefer the statistically poorer fits if the wavelength of the peak of the modelled silicate absorption or emission feature is better centred on the observed feature. Such discrepancies arise because the Trapezium and μ Cephei emissivities cover slightly different wavelength ranges, i.e. 8.1–12.8 and 8.4–13.3 μm , respectively.

4.5.1 Inner and outer dust temperatures, T_0 and T_D or T_S

In preliminary fits to the TMC sources with 40 annuli, flux contributions from components hotter than 1000 K each contributed ≤ 0.1 per cent at 10 μm , whilst the fluxes owing to annuli for which $T < 70$ K were too small to calculate; hence the temperatures of the inner and outer annuli, T_0 and T_D (or T_S), were set to 1000 and 70 K, respectively, as in Paper I.

However, fits to ρ -Elias 29 resulted in physically unrealistic values of q_d (1.5 and 6.0, for fits with the μ Cephei and Trapezium emissivities, respectively). Inspection of the annular flux components indicated that such discrepancies arose when the flux of the 1000-K annulus exceeded 1 per cent of the total disc or sphere flux. For ρ -Elias 29 and 23 and FU Ori, increasing T_0 to 2000 K and the number of annuli to 80 to keep a similar temperature increment, resulted in physically realistic values of q_d and better quality

Table 2. Disc model fits to the 10- μ m spectra. Preferred fits are typed in bold (fits with peak wavelength closest to that of the observations). Fits with the lowest χ^2_{ν} are italicized if they are not the same as the preferred fits. Tabulated values of $c_{\text{sil}} = 0.00$ indicate that this parameter was fixed at that value, fits to T-Elias 18 and V645 Cyg were stable only when they were forced to be optically thick.

Source	T_* (kK)	A_V (mag)	Trapezium			μ Cephei			$\tau_{10} < 1$
			q_d	c_{sil}	χ^2_{ν}	q_d	c_{sil}	χ^2_{ν}	
Low-mass YSOs									
Quiescent environments									
T-HL Tau	4.0	23	0.44	1.1	9.1	0.53	0.56	15	✓
T-Elias 18 ^a	15	17	–	0.47	2.7	–	0.34	6.0	×
T-Elias 7N	4.0	6-10	0.33	1.7	24	<i>0.34</i>	<i>1.1</i>	23	×
		30	0.34	1.7	24	<i>0.35</i>	<i>1.1</i>	23	
T-T TauS	4.0	5	0.46	1.0	8.0	<i>0.52</i>	<i>0.55</i>	<i>6.4</i>	✓
		10	0.48	1.0	8.0	<i>0.53</i>	<i>0.55</i>	<i>6.4</i>	
		22	0.50	1.0	8.2	<i>0.57</i>	<i>0.55</i>	<i>6.5</i>	
T-Haro 6-13	4.0	9.5	0.36	0.00	0.93	<i>0.39</i>	<i>0.00</i>	<i>0.79</i>	×
F-V1057 Cyg ^b	5.1	3.6	0.40	0.00	3.4	0.42	0.00	4.0	×
V536 Aql	4.0	3.6	0.32	0.00	1.8	0.40	0.00	2.0	✓
F-V1515 Cyg	5.0	2.8	0.36	0.00	1.6	0.42	0.00	1.8	✓
F-V1331 Cyg	6.0	2.4	0.32	0.00	0.88	0.38	0.00	0.92	✓
T-HP Tau	4.7	2.26	0.32	0.00	1.3	0.43	0.00	1.4	✓
T-SU Aur	5.7	1.45	0.23	0.00	12	0.33	0.00	5.3	✓
T-V773 Tau	4.7	1.32	0.35	0.47	1.5	0.45	0.26	1.3	✓
T-DK Tau	4.0	1.3	0.23	0.30	3.5	0.24	0.76	2.6	✓
DI Cep	5.0	0.9	0.16	0.00	4.6	0.23	0.00	1.6	✓
Disrupted environments									
ρ -Elias 29 ^c	4.0	47	1.0	1.7	10	0.83	1.3	9.9	×
ρ -Elias 21	3.4	22.6	0.34	1.1	3.6	0.37	0.73	2.7	×
ρ -Elias 23 ^c	4.0	10.2	0.23	1.5	1.5	0.58	0.64	1.2	×
ρ -Elias 28	4.9	3.9	0.23	0.00	2.5	0.32	0.00	2.1	✓
F-FU Ori ^c	5.5	2.2	0.53	0.00	3.0	0.54	0.00	1.6	×
Herbig AeBe stars									
V645 Cyg	9.7	2.6	0.51	0.50	2.2	0.50	0.38	1.9	×
LkH α 233	7.9	2.6	0.35	0.63	1.4	0.43	0.26	1.9	✓
WW Vul	8.6	2.2	0.20	0.00	2.3	0.37	0.00	1.5	✓
LkH α 208	13	1.7	<i>0.23</i>	<i>0.00</i>	<i>1.8</i>	0.44	0.00	1.9	✓
HD 150193 ^c	8.8	1.61	0.28	0.00	17	0.54	0.00	38	✓

^aThe model was truncated at $T_D = 600$ K. ^bSpherical model fits with the Trapezium emissivity produced a weak silicate absorption feature. The parameters of this fit were $q_s = 0.58$, $c_{\text{sil}} = 0.090$ and $\chi^2_{\nu} = 3.4$. ^c $T_0 = 2000$ K.

fits. For low-mass YSOs with $q_d \lesssim 0.5$ and a smaller 1000-K flux component, increasing T_0 reduced q_d and q_s by $\lesssim 8$ and $\lesssim 12$ per cent, respectively (the discrepancy increased with the value of the temperature index), and did not change the fit or the continuum. Fits to the most optically thin Herbig AeBe stars, WW Vul and HD 150193 were significantly better with $T_0 = 2000$ K models even though their disc temperature indices with the 1000-K model were below 0.5. T-Elias 18, was fitted with models truncated at ~ 600 K (see Section 4.9).

4.6 Comparison between disc and sphere models

In the majority of cases the qualities of fits obtained with the spherical model were identical to those obtained with the disc morphology. Differences in the qualities, χ^2_{ν} of the fits with the two models was $\lesssim 5$ per cent for all sources except F-FU Ori (7 per cent) and T-SU Aur (9 per cent); in both cases the disc model fits were better. We judge these differences to be insignificant because χ^2_{ν} variations between the two models do not correlate with changes in the fits or the continua. In most cases the continua obtained with the two

models were identical; where continua differed slightly between the disc and spherical models both continua are shown in the plots. The only significant difference was seen for ρ -Elias 23; for this object the continuum produced by the spherical model and the Trapezium emissivity was 25 per cent larger than that obtained with the disc. However, the fit with the narrower μ Cephei silicate feature was significantly better. The most likely cause of the discrepancy between the disc and spherical fits is the large uncertainty in the flux near the peak of silicate absorption in this observation. Other authors (e.g. Gledhill & Yates, in preparation) have shown that in order to discriminate between spherical and disc models multiwavelength images are required, such as that provided by UKIRT in the near-infrared (NIR) and GEMINI/VLT in the MIR. This applies to radiative transfer models as well as the simple models used in this work.

4.6.1 q_s versus q_d

The fitted values of the spherical (q_s) and disc (q_d) temperature indices of the 23 modelled spectra are plotted in Fig. 2(a); the dotted

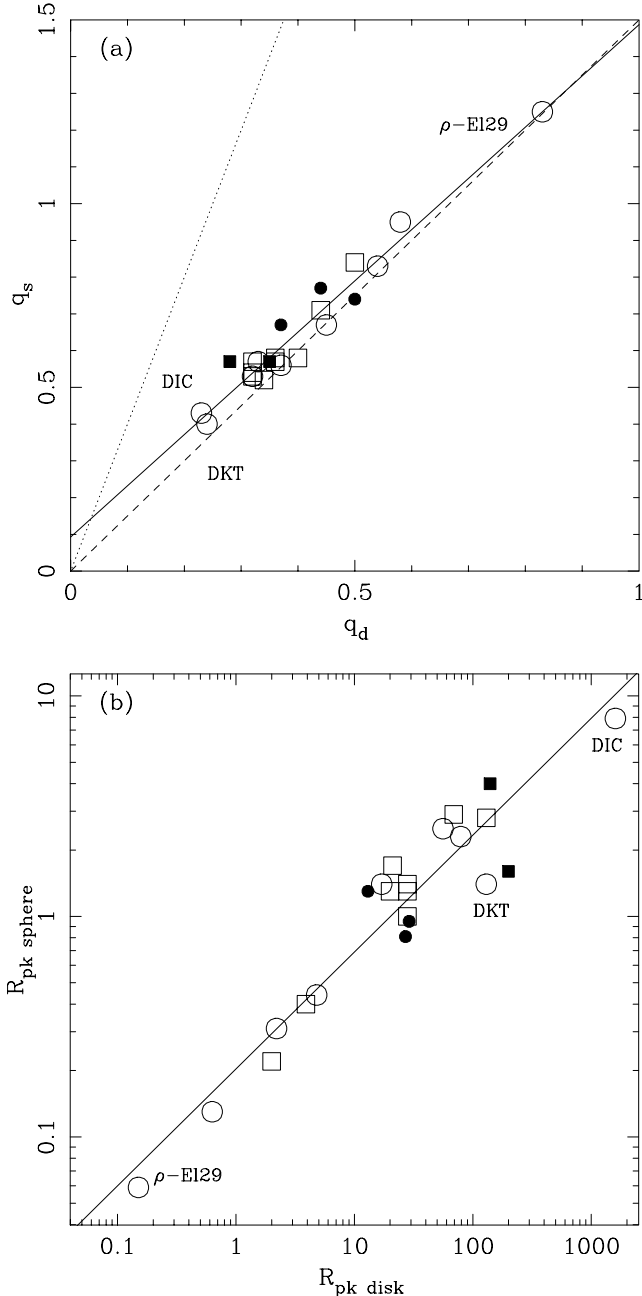


Figure 2. q_s versus q_d and $R_{\text{pk sphere}}$ versus $R_{\text{pk disc}}$. (a) The spherical temperature index $q_s = 0.09 \pm 0.03 + (1.39 \pm 0.07)q_d$, where q_d is the disc temperature index (solid line); with a Pearson correlation coefficient of 0.97 for 23 data points. Dashed and dotted lines show, respectively, the analytical relationship for optically thick and optically thin discs. (b) Comparison between the modelled sphere and disc radii, for the largest flux component at $10.0 \mu\text{m}$. The best-fitting straight line to the data is $\log R_{\text{pk sphere}} = -0.69 \pm 0.06 + (0.53 \pm 0.04)\log R_{\text{pk disc}}$ and the Pearson correlation coefficient is 0.95 for the 23 data points. Filled and empty symbols represent Herbig AeBe stars and low-mass T Tauri stars, respectively; sources for which the $10\text{-}\mu\text{m}$ spectra were better fitted with the Trapezium molecular cloud emissivity are indicated by squares; μ Cephei fits are indicated with circles.

and dashed lines in the figure represent the relationship between these parameters in the optically thin ($q_s \approx 4q_d$) and optically thick ($q_s \approx 3/2q_d$) limits. The linear fit to the modelled data (solid line) is $q_s = 0.09 \pm 0.03 + (1.39 \pm 0.07)q_d$, close to the analytical

value in the optically thick limit. DK Tau and DI Cep, which were marginally better fitted with the spherical model, have very low disc temperature indices of 0.24 and 0.23, respectively. The estimated disc radius for DI Cep is extraordinarily large at 1600 au (more than 10 times larger than any other member of the sample), whilst the radius of the sphere is 8 au (2.5 times that of any other source). In the case of DK Tau the low-temperature index may be a consequence of the poor quality of the spectrum.

Because fits with the spherical model did not differ significantly from those with the disc model, and independent observations associate most of the objects with a disc morphology, we shall discuss only the disc model results in the remainder of this paper.

4.7 Visual extinction, silicate absorption and q_d

Foreground silicate absorption features were essential in models of the most highly extinguished sources in the TMC and the ρMC (T-HL Tau, T-Elias 18, T-Elias 7, T-T Tau, ρ -Elias 29, ρ -Elias 21 and ρ -Elias 23), and the most optically obscured Herbig AeBe stars (V645 Cyg and LkH α 233). In addition we obtained marginally better fits to the less-obscured sources T-DK Tau and T-V773 Tau ($A_V \sim 1.3$) when a silicate absorption feature was included in the models. However, this may be spurious due to the low S/N ratio of these data. Disc models for T-V773 Tau that excluded silicate absorption features were only slightly poorer ($\chi^2_\nu = 1.6$ instead of 1.5) and produced higher temperature indices ($q_d = 0.52$ instead of 0.45). These CGS3 data are probably insensitive to weak absorption features ($c_{\text{sil}} \lesssim 0.3$). Assuming the higher A_V values for T-Elias 7N and T-T TauS derived in Section 4.8, below and interpolating between the data for quiescent and disrupted regions (Fig. 3) silicate absorption with an optical depth $\gtrsim 0.3$ could have been detectable towards low-mass YSOs when the visual extinction exceeds ~ 10 mag; for Herbig AeBe stars the current lower limit for this amount of silicate absorption is $A_V \gtrsim 2.2$ mag. The extinction limit for measurable silicate absorption is probably lower in Herbig AeBe stars. This is because the disc atmosphere intercepts a smaller fraction of the light from the stellar photosphere, thus disc flaring is less important than in the low-mass T Tauri and FU Ori stars so that light from the photosphere is less scattered; also there is negligible foreground molecular cloud material.

4.8 Extinction towards known TMC binaries

The relationship between visual extinction and the optical depth of the modelled silicate absorption feature for the TMC is plotted in Fig. 3(a); for the most highly extinguished objects, Elias 18 and HL Tau the degree of silicate absorption increases with the visual extinction. However, for the Elias 7 and T Tau systems the silicate absorption is excessive in comparison to Elias' (1978) near-infrared A_V estimates based on the assumption that each was a single source. More recent, spatially resolved measurements show that the near-infrared and $10\text{-}\mu\text{m}$ flux of these systems are dominated by different components of the system (see Paper I for Elias 7 and Appendix A1.2 for T Tau). The extinction towards Elias 7 is consistent with the relationship between the optical depth of the $3.1\text{-}\mu\text{m}$ H $_2$ O ice band and A_V (Fig. 4a). The modelled $10\text{-}\mu\text{m}$ spectra of T Tau S and Elias 7 N were obtained after subtracting estimated fluxes caused by the optical primaries (T Tau N and Elias 7 S). Using the Haro 6–13, Elias 18 and HL Tau silicate optical depths, we estimate that the true visual extinction estimates are nearer 30 mag for Elias 7N and 22 mag for T Tau S, whilst the visual extinctions towards the primaries are consistent with Elias' estimates.

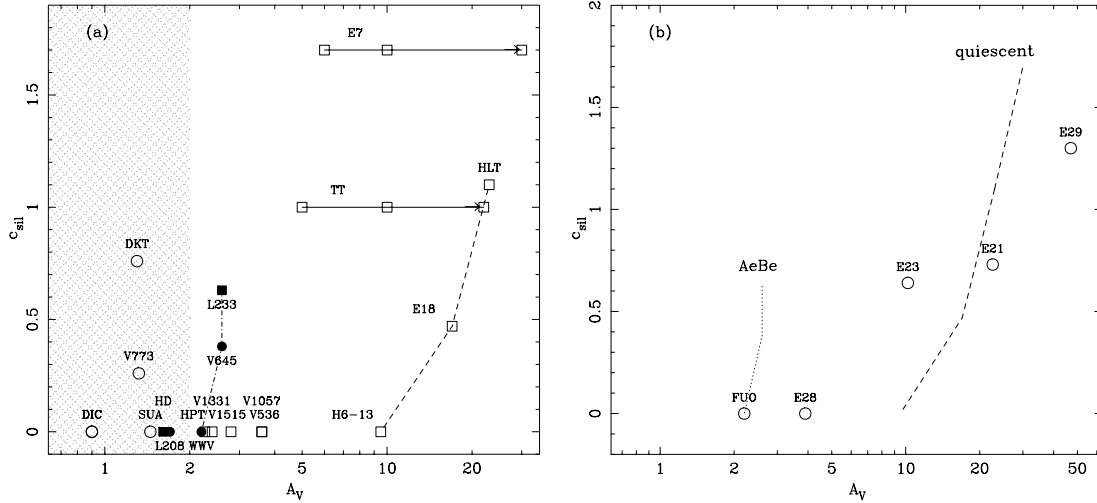


Figure 3. Fitted silicate optical depths plotted against visual extinction (a) for low-mass YSOs and Herbig AeBe stars in quiescent environments and (b) for low-mass YSOs and Herbig AeBe stars in disrupted environments. The hatched area in (a) denotes the A_V range for low-mass objects, which were better matched by the μ Cephei emissivity, dot-dashed and dashed lines, respectively, show the relationship between A_V and $c_{\text{sil}} \geq 0$ for Herbig AeBe stars and low-mass YSOs in quiescent molecular clouds excluding the low-S/N ratio sources DK Tau and V773 Cyg (see Section 4.7); solid lines indicate the range of A_V determined for the T Tauri and Elias 7 binaries and lines with arrows indicate the newly inferred extinctions towards T Tauri S and Elias 7N (Section 4.8). The dotted and dashed lines, respectively, show the relationship between A_V and $c_{\text{sil}} \geq 0$ for Herbig AeBe stars and YSOs in quiescent molecular clouds. The key to the plotting symbols is in Fig. 2.

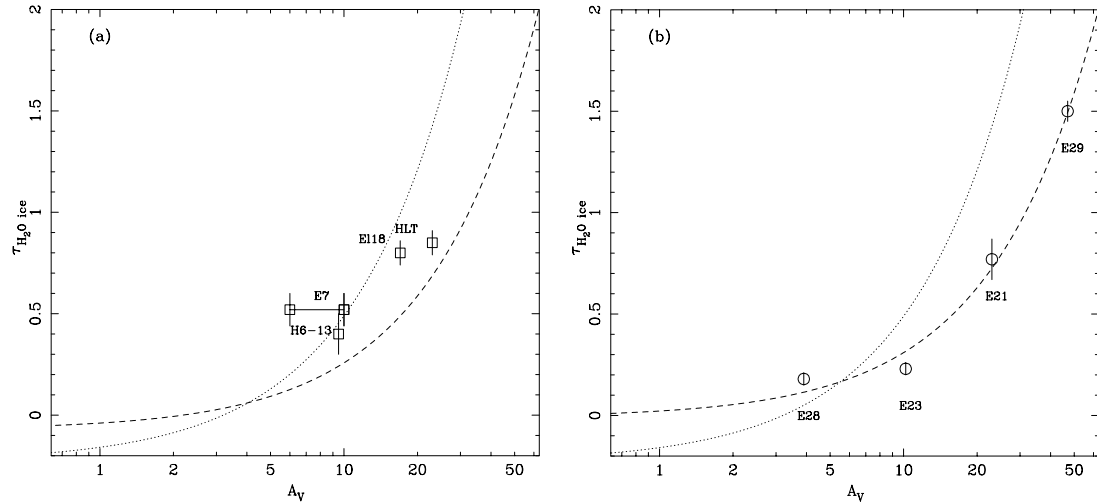


Figure 4. $3.1\text{-}\mu\text{m}$ H_2O -ice band optical depths in comparison with visual extinction for low-mass stars (a) in the quiescent TMC (Whittet et al. 1988) and (b) the disrupted ρ MC (Tanaka et al. 1990). The dotted curves represent the relationship between $\tau_{\text{H}_2\text{O}}$ and visual extinction for field stars obscured by the TMC: $\tau_{\text{H}_2\text{O}} = 0.072(A_V - 3.2)$, obtained by Whittet et al. (2001). In (a) plotted values of $\tau_{\text{H}_2\text{O ice}}$ and A_V for T-Elias 7 probably reflect that of the primary, whilst c_{sil} probably reflects that of the secondary (see Section 4.8); the dashed curves represent the weighted fits to data for the four ρ MC YSOs, $\tau_{\text{H}_2\text{O ice}} = 0.032 \pm 0.001(A_V - 0.31 \pm 0.83)$ with a correlation coefficient = 0.99. See Fig. 2 for a key to plotting symbols.

For Elias 7N, increasing A_V to 30 mag produces a negligible change in q_d (+3 per cent; Table 2), but the disc is 49 per cent of the size for $A_V = 6$ mag (Table 3). In Paper I we discussed the good agreement between our derived disc sizes and the NIR emission observed by Ménard et al. (1993). The projected separation of the binary is 175 au; therefore in the high- A_V limit the $10\text{-}\mu\text{m}$ emission is probably derived from a circumstellar rather than a circumbinary disc. For T Tau S increasing A_V from 5 to 22 mag increased the temperature indices by ~ 10 per cent and decreased the disc radius by 30 per cent.

4.9 Fits to T-Elias 18 with truncated models

The $10\text{-}\mu\text{m}$ spectrum of Elias 18 (IC 2087) is peculiar because it shows a strong silicate absorption feature on a falling photosphere-

like continuum, implying that the source is a field star behind the TMC. However, Elias' (1978) near-infrared photometry indicates that the object is embedded in the TMC with an unusually early spectral type (B5) for a YSO in this association and substantial visual extinction ($A_V \sim 17$ mag). More recently Shuping et al. (2001) observed CO bandhead emission at $2.3\text{ }\mu\text{m}$ from the inner 1800–5000 K regions of a circumstellar disc but they infer a very low visual extinction ($A_V < 1$). We prefer fits obtained with $A_V \sim 17$ because the optical depths of the $3.1\text{-}\mu\text{m}$ H_2O ice band correlates well with that for other highly obscured YSOs.

The $10\text{-}\mu\text{m}$ spectrum of Elias 18 is not well represented by a single reddened blackbody (e.g. Whittet et al. 1988). Bowey et al. (1998) fitted the $10\text{-}\mu\text{m}$ spectrum of Elias 18 with a physically unrealistic three-component model in an attempt to simulate the

Table 3. Physical results of the 10- μm disc model. Radii are based on $R_* = 2.0 R_\odot$. For AeBe stars the median is 2.1 (Mannings & Sargent 1997) but these models use 2.0.

Object	ϵ_v	Pre-set		F_{pk} (Jy)	ΔT (K)	Disc parameters ^a			
		T_* (kK)	A_V (mag)			$T(F_{\text{pk}})$ (K)	$\Delta\tau_{\text{em}}$	R_{pk} (au)	R_{sil} (au)
Low-mass YSOs									
Quiescent environments									
T-HL Tau	Trap	4.0	23	0.95	200–550	308	0.51–24	3.9	11
T-Elias 18	Trap	15	17	0.39	600–860	600	∞	–	–
T-Elias 7	Trap	4.0	6	2.2	150–360	213	0.97–100	110	410
			10	2.2	150–370		1.0–110	99	350
			30	2.4	140–390		1.0–100	69	200
T-T Tau	Trap	4.0	5	2.9	200–600	332	0.60–25	3.0	6.3
			10	2.9	210–620		0.59–25	2.0	5.4
			22	3.5	160–600	285	4.0–320	2.0	6.6
T-Haro 6-13	Trap	4.0	9.5	0.11	180–440	261	2.0–32	20	63
F-V1057 Cyg	Trap	5.1	3.6	0.63	170–460	261	1.0–63	21	66
V536 Aql	Trap	4.0	3.6	0.22	200–400	308	0.25–16	28	100
F-V1515 Cyg	Trap	5.0	2.8	0.19	200–470	308	0.32–20	28	100
F-V1331 Cyg	Trap	6.0	2.4	0.079	210–470	308	0.20–13	130	450
T-HP Tau	Trap	4.7	2.26	0.12	230–540	356	0.11–10	28	130
T-SU Aur	μ Cep	5.7	1.45	0.33	230–520	356	0.15–10	56	240
T-V773 Tau	μ Cep	4.7	1.32	0.18	200–550	308	0.63–32	4.8	14
T-DK Tau	μ Cep	4.0	1.3	0.29	260–620	452	0.01–5	130	1500
DI Cep	μ Cep	5.0	0.9	0.23	220–460	332	0.040–7.9	1600	10 ⁴
Disrupted environments									
ρ -Elias 29	μ Cep	4.0	47	1.3	220–1180	436	∞	0.15	0.36
ρ -Elias 21	μ Cep	3.4	22.6	1.3	130–420	237	4.0–660	17	83
ρ -Elias 23	μ Cep	4.0	10.2	0.17	220–740	339	1.0–40	0.71	1.8
ρ -Elias 28	μ Cep	4.9	3.9	0.23	200–440	285	0.25–16	79	280
F-FU Ori	μ Cep	5.5	2.2	0.34	200–660	314	1.3–63	2.2	5.6
Herbig AeBe stars									
V645 Cyg	μ Cep	9.7	2.6	6.3	160–600	285	∞	13	48
LkH α 233	Trap	7.9	2.6	0.71	190–440	285	0.40–25	140	500
WW Vul	μ Cep	8.6	2.2	0.14	280–740	485	0.063–6.3	27	140
LkH α 208	μ Cep	13	1.7	0.26	250–680	404	0.21–10	29	90
HD 150193	Trap	8.8	1.61	1.4	300–880	583	0.0050–4.0	200	2500

^a ΔT and $\Delta\tau_{\text{em}}$ are, respectively, the ranges of annular temperature and 10.0 μm emission optical depths for which $F_{\text{annulus}} \geq e^{-1} F_{\text{pk}}$; R_{pk} is the outer radius of the annulus which produces the largest flux component at 10.0 μm ; R_{sil} is the outer radius of the *silicate* disc where $F_{\text{annulus}} = e^{-1} F_{\text{pk}}$.

presence of a photosphere, single temperature optically thick dust emission at 1000 K, and 150-K optically thin emission,² which produced a continuum with a kink at 11.0 μm and resulted in excess absorption in the silicate absorption profile. Our standard disc and sphere models with $T_{\text{outer}} = 70$ K also resulted in poor fits with very optically thin silicate emission and very strong foreground absorption features ($c_{\text{sil}} \sim 2$) (dashed curves in Fig. 5). Good fits could be obtained only with optically thick discs or spheres in which the temperature of the largest 10- μm flux component was between 500 and 600 K. For both the $T_0 = 1000$ K models this occurred when the temperature of the coolest annulus was set to 600 K and $q_d = 0.50$. For the 2000-K model the best fit was obtained with T_D in the 500–600 K range and $q_d = 0.33$ (600 K) – 0.55 (500 K); 2000–70 K fits were only slightly poorer $\chi^2 = 2.8$, but produced unrealistically high values of $q_d = 1.2$. We concluded that q_d values were fitted to minimize the low-temperature (70–500 K) flux contribution and to maximize the 600–800 K components; since the q_d of Elias 18 is poorly constrained by fits to its 10- μm spectrum we cannot infer a physical size for its 10- μm -emitting region.

²The 250-K value quoted by Bowey et al. is in error.

5 ENVIRONMENTAL EFFECT ON THE YSOs

Our models suggest that the properties of Herbig AeBe stars and low-mass YSOs in quiescent environments are similar. However, there are distinct differences between the modelled disc and dust properties of low-mass YSOs in quiescent and disrupted environments.

5.1 Modelled emission features

Following the method of Paper I we define the range in temperature and optical depth of significant annular flux components to be those for which $F_{\text{annulus}} \geq F_{\text{pk}}/e$. F_{pk} is the largest annular flux component at 10.0 μm and e is the base of natural logarithms; the values are given in Table 3.

Fits indicate that 10 out of 14 of the quiescent-region low-mass YSOs and four out of five of the Herbig AeBe features contain an optically thin silicate emission component. However, four out of five of the disrupted-region YSOs are optically thick at 10 μm . We obtain optically thick 10- μm emission for V645 Cyg and ρ -Elias 29 in agreement with the spectropolarimetric measurements by Smith et al. (2000). Unfortunately, no 10- μm spectropolarimetry exists for the other sources.

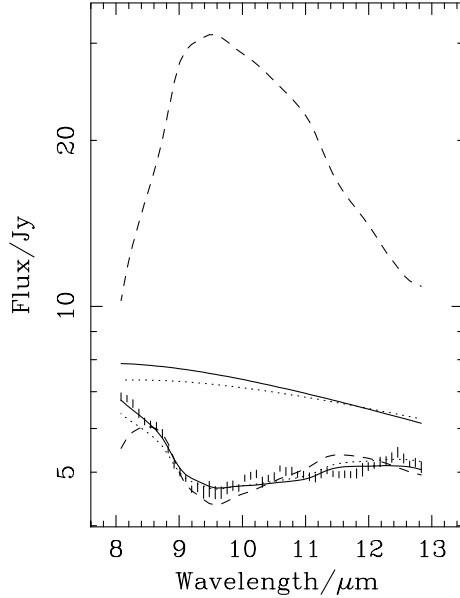


Figure 5. Comparison between models for Elias 18 (error bars) with normal ($T_{\text{outer}} = 70$ K) and truncated discs. Solid curves – best fit ($\chi^2_{\nu} = 2.7$) and continuum obtained with an optically thick disc, which was truncated at 600 K; dashed and dotted curves – optically thin ($\chi^2_{\nu} = 15$) and optically thick ($\chi^2_{\nu} = 5.1$) fits and continua obtained with the normal disc model.

As found in Paper I, models for the spectra of quiescent-region low-mass YSOs are most sensitive to temperatures in the ~ 200 – 400 K range. For the Herbig AeBe stars the contributing temperature range is generally larger (~ 200 – 800 K) because the flux contribution of each annulus is smaller in comparison to the total flux. Preliminary fits with $T_0 = 1000$ K indicated flux contributions from an even wider range of temperatures (200 to >1000 K) for ρ -Elias 29 and 23; therefore we changed T_0 to 2000 K. These hotter models produced significant flux components up to 1180 K for ρ -Elias 29 and 750 K for ρ -Elias 23. The spectrum of T-Elias 18 was dominated by flux temperatures in the 600–800 K range because it was fitted with a truncated disc (see Section 4.9).

5.2 Fitted disc temperature indices

Fits of the disc temperature index, q_d , to the 13 spectra of low-mass YSOs in quiescent environments are in the range 0.23–0.50 with a mean and standard deviation of 0.35 ± 0.07 and those to Herbig AeBe stars are 0.28–0.50 with a mean value of 0.39 ± 0.08 . These values indicate that the emission arises from optically thin layers above an optically thick disc and/or that the temperature index is modified by the effects of grain condensation and evaporation (see Section 1). In contrast the disc temperature indices of sources in disrupted ρ MC and F-FU Ori environments cover a wider range. Elias 21 and Elias 28 have quiescent-region temperature indices of 0.37 and 0.32, respectively. However, for FU Ori, Elias 23 and Elias 29 the fitted values of q_d are higher (0.54, 0.58 and 0.83, respectively). Elias 29 ($q_d = 0.83$) is the only source with a temperature index indicative of a flat optically thick disc $q_d \sim 0.75$.

5.3 Apparent sizes of the discs at 10 μm

As in Paper I we define the radius of the disc when $\lambda = 10$ μm , R_{sil} , to be that where the flux falls below F_{pk}/e , where e is the base of natural logarithms; thus the radius of peak 10- μm emission is R_{pk} . It is important to remember, however, that these sizes depend critically

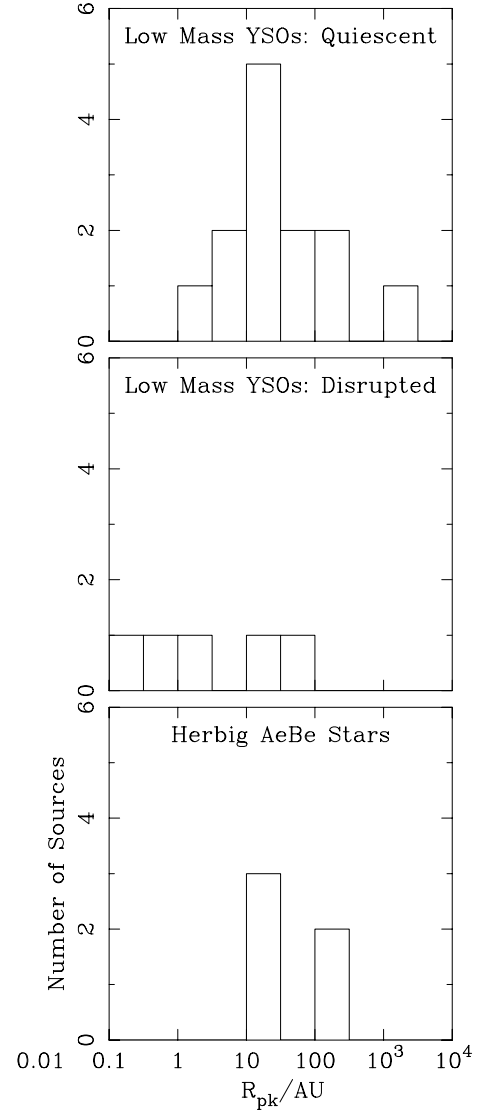


Figure 6. Histogram of disc radii for the sample. R_{pk} is the radius of the disc for the largest flux component at 10 μm .

on parameters that are difficult to determine for embedded objects, namely the estimated photospheric temperature, stellar radius and A_V , with the largest uncertainty in A_V .

The galactic environment seems to have a stronger effect on constraining the radius of the surface layers of the dust disc than does the temperature and mass of the photosphere. The radii of the peak 10- μm emission for the majority (nine out of 13) of the quiescent-region low-mass YSOs and the five Herbig AeBe stars is in the 10–140 au range (Fig. 6 and Table 3). However, the discs of the small sample of YSOs from disrupted galactic environments seem to be more compact: none of the sample is larger than 80 au and three out of five are $\lesssim 2$ au in size. This inferred difference in disc size between quiescent-region and disrupted-region low-mass YSOs is also observed at 1.3 mm (see Section 3.2.1).

6 GRAIN PROPERTIES

6.1 Feature contrast in the modelling emissivities

The modelling emissivities used in this (and most other) studies of interstellar silicates are based on observations of dust emission in

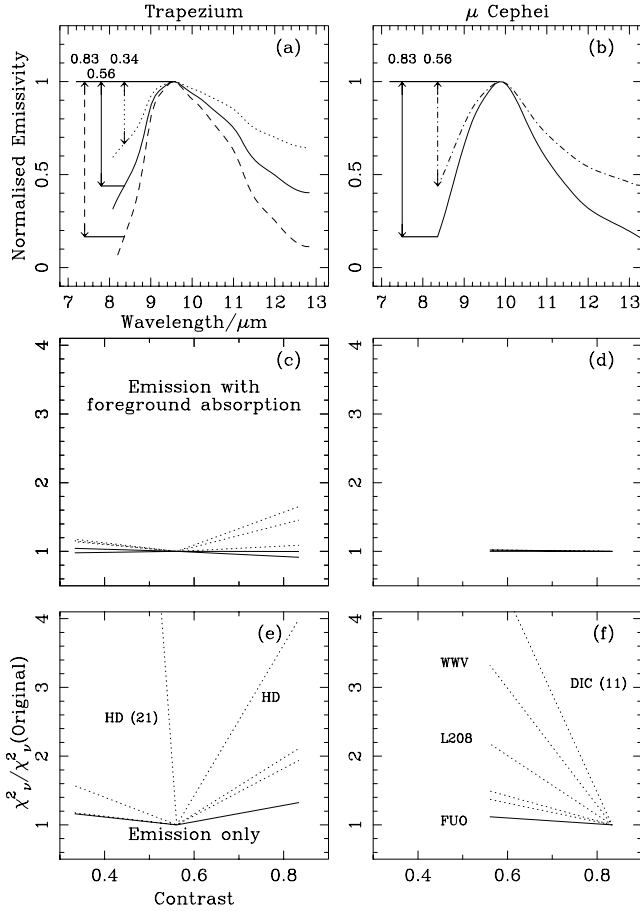


Figure 7. Fit quality as a function of the contrast in the modelling emissivity. (a) and (b) arrows indicate the contrasts in the features evaluated at $8.36\ \mu\text{m}$. Solid curves are the original Trapezium and μ Cephei emissivities, which have contrasts of 0.56 and 0.83, respectively; the dashed curve is the Trapezium shape scaled to the contrast of the original μ Cephei emissivity at $8.36\ \mu\text{m}$, the dotted curve is the Trapezium emissivity scaled to a lower contrast, the dot-dashed curve is the μ Cephei emissivity scaled to that of the Trapezium. Parts (c)–(f) show the effect of contrast changes on the ratio of χ^2_v to that obtained with the original better fitting emissivity for objects with good $10\text{-}\mu\text{m}$ spectra. Solid and dotted lines indicate values for optically thick and optically thin emission features, respectively.

two fundamentally different calibrating sources: the Orion Trapezium (Forrest et al. 1975) and μ Cephei (Russell et al. 1975) (solid curves in Figs 7a and b). These two emissivities are quite distinct in shape, peaking at wavelengths of 9.6 and $9.8\ \mu\text{m}$, respectively, and the Trapezium feature contains a shoulder centred at $10.8\ \mu\text{m}$. However, there is also a considerable difference in their degrees of contrast; the Orion emissivity retains a value of ~ 0.4 at the edges of the normalized band, whereas the μ Cephei feature $\lesssim 0.2$ at 8.4 and $13\ \mu\text{m}$. Both emissivities are derived by dividing the observed spectrum by a 250-K blackbody. However, prior to this a substantial photospheric component was subtracted from the μ Cephei spectrum. Uncertainties in the level of the photospheric component would artificially enhance or reduce the contrast in the resulting emissivity.

The current sample offers an independent check on the reality of the difference between these two standards. Changes in the feature contrast did not cause profiles that were better matched by the Trapezium to be better fitted by the μ Cephei profile; however, contrast variation did change the quality of the fits (Figs 7c–f). In

sources with optically thin emission and foreground silicate absorption, which were fitted with the Trapezium emissivity (dotted lines in Fig. 7c) a convincing minimum in the ratio of χ^2_v of the fit with scaled emissivity to the emissivity of the standard emissivity is seen, not far from the assumed contrast of 0.56. Optically thick sources (solid lines) show smaller changes because the shape of the silicate profile affects only the modelled absorption feature. Fig. 7(d) shows the effect of scaling the μ Cephei emissivity to the contrast of the Trapezium: the ratio of the fitted qualities is essentially constant, for both optically thick and optically thin sources with foreground silicate absorption. Finally, Figs 7(e) and (f) show the same variation for sources with no foreground absorption features; again the best fits to the observed spectra were obtained with contrasts close to the standard values in both the Trapezium and μ Cephei emissivities, confirming that the assumed excess in the level of the standard Trapezium profile relative to the μ Cephei emissivity is real.

6.2 Best-fitting silicate emissivities

Our results are different from those of HBT1995 and HBT1998, who found with much simpler models that the Trapezium emissivity was always a better match to the data than μ Cephei, but that ρ -Elias 21, T-HL Tau, T-T Tau S were narrower than the Trapezium feature.

6.2.1 Visual extinction and silicate mineralogy in quiescent-region YSOs

Better fits to the $10\text{-}\mu\text{m}$ spectra of low-mass quiescent-region YSOs, the visual extinction of which exceeds 2.26 mag are obtained with the broader Trapezium emissivity. In contrast the spectra of less obscured sources with $A_V \lesssim 1.45$ mag are better matched by the narrower profile of silicates surrounding μ Cephei. Since the Trapezium emissivity represents processed molecular cloud dust and μ Cephei dust is newly condensed circumstellar dust, the observed change in the silicate profile at $A_V \sim 2$ mag is indicative of a change in the mineralogy of the dust. Since both types of silicate feature are present in absorption and emission spectra we attribute these differences to the silicate mineralogy and not to the presence or absence of icy grain mantles, or to changes in grain size.

6.2.2 μ Cephei-like silicates in disrupted-region YSOs

The spectral properties of YSO silicates in the ρ MC and FU Ori differ significantly from those of low-mass stars in quiescent environments. Despite the wide range in visual extinction ($2.2\text{--}47$ mag) the spectra of these five sources are better matched by models with the narrow μ Cephei circumstellar emissivity than they are with the Trapezium silicate profile.

6.2.3 Herbig AeBe stars

LkH α 233 and HD 190153 are both located in molecular clouds and are best matched with the Trapezium emissivity. In contrast, V645 Cyg, LkH α 208 and WW Vul are not located in molecular clouds and their silicate profiles are fitted better with the circumstellar μ Cephei emissivity. However, the sample and extinction range are insufficiently large to know whether the results for these five sources can be generalized to other Herbig AeBe stars.

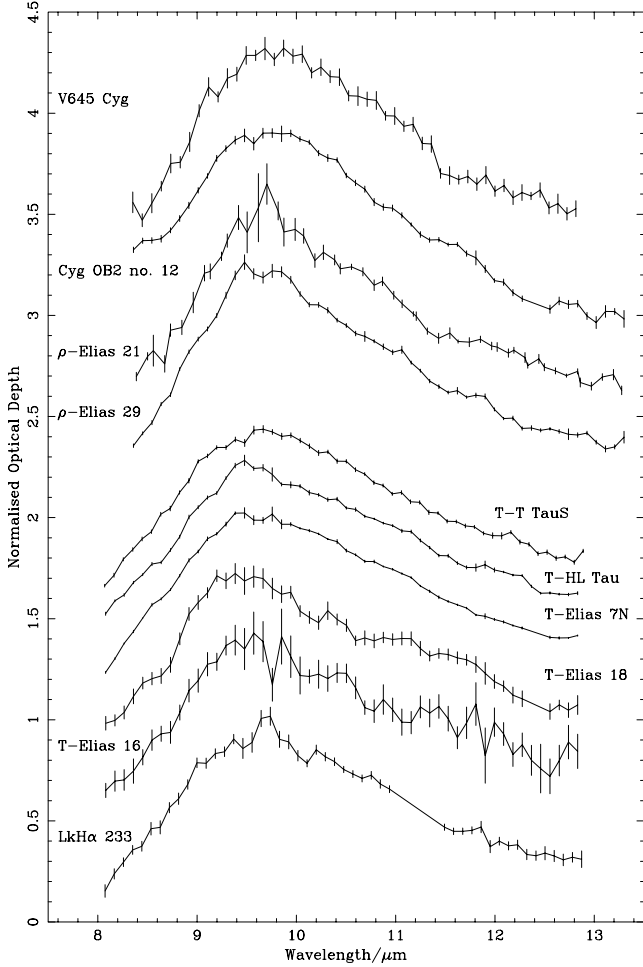


Figure 8. Normalized silicate absorption profiles of YSOs compared with silicate profiles for lines of sight through quiescent regions of the TMC towards T-Elias 16 and through the diffuse ISM towards Cyg OB2 no. 12 from Bowey et al. (1998); the offsets in the y-axis are -0.1 (LkH α 233), 0.4 , 0.7 , 1.0 , 1.25 , 1.4 , 2.2 , 2.5 , 2.9 and 3.3 (V645 Cyg).

6.3 Silicate absorption and emission profiles

Silicate absorption profiles were derived from the observations and continua estimated with the disc model (see Fig. 1); the normalized optical depth profiles of the highest S/N ratio absorption features are plotted in Fig. 8. As suggested above the silicate absorption features towards ρ -Elias 21 and 29 and V645 Cyg are similar in width and peak wavelength to the profile of diffuse ISM dust in the line of sight towards Cyg OB2 no 12, whilst the absorption profiles towards the TMC sources are similar to the absorption through the quiescent molecular cloud towards the field star T-Elias 16.

The peak wavelength (λ_c) and FWHM of the silicate absorption and most optically thin emission profiles³ are compared with those for a variety of dusty environments in Fig. 9. As expected, profiles that were better fitted with the μ Cephei emissivity appear in the top left-hand side of the figure, those that were better matched by the Trapezium fall in the bottom right.

³The FWHM of the normalized emission features was derived by assuming that the optical depth near $8.0 \mu\text{m}$ was similar to that of the better-fitting emissivity: μ Cephei [$\tau(8.4 \mu\text{m}) \approx 0.2$] or the Trapezium [$\tau(8.1 \mu\text{m}) \approx 0.3$].

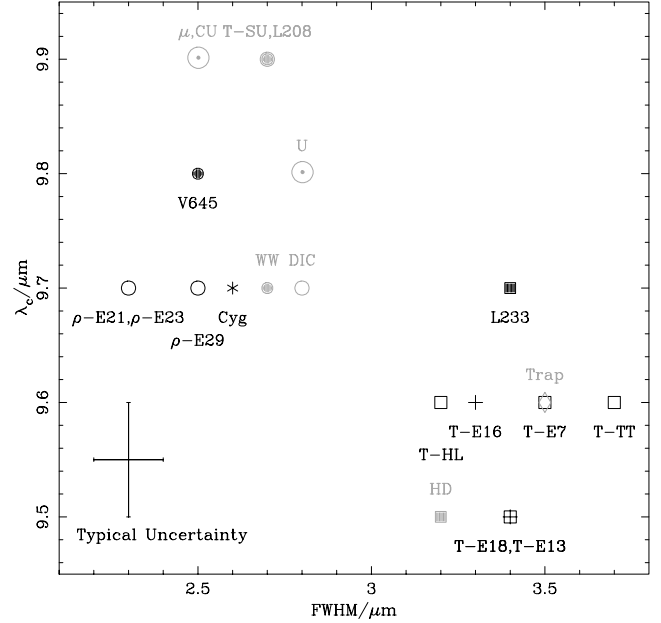


Figure 9. Peak wavelength versus FWHM of the derived silicate absorption features (black) and optically thin silicate emission features (grey). The key to the plotting symbols for low-mass YSOs and Herbig AeBe stars is in Fig. 2, additional source types- dust in the diffuse ISM towards Cyg OB2 no. 12 (*) and the TMC (+), circumstellar silicate emission features around evolved stars (\odot) (see Bowey & Adamson 2002). For ρ -Elias 23 and T-SU Aur the typical uncertainty should be doubled.

Comparisons between the FWHM and peak wavelength of the most optically thin $10\text{-}\mu\text{m}$ YSO emission features, the absorption features and with those of a variety of astronomical environments (see Bowey & Adamson 2002) indicate a bimodal population of silicate features: features that peak near $9.8 \mu\text{m}$ are relatively narrow (FWHM $\sim 2.6 \mu\text{m}$), whilst those that peak near $9.6 \mu\text{m}$ have a FWHM $\sim 3.4 \mu\text{m}$. We attribute the increased width and decreased peak wavelength of the quiescent molecular cloud profiles to an increase in the pyroxene content of the dust (both crystalline and amorphous) rather than grain size (see Bowey & Adamson 2002).

6.4 Discussion

6.4.1 Silicate mineralogy and the TMC H_2O ice-band threshold

Studies of the $3.1\text{-}\mu\text{m}$ H_2O ice absorption feature towards field stars behind the TMC show that the feature is observed only when $A_V \gtrsim 3$ mag (e.g. Whittet et al. 1988, 2001) and a correlation with A_V (see the dotted curves in Fig. 4). Since the ice-band threshold is close to the $A_V \sim 4$ mag threshold at which there is a change in the dependence of C^{18}O on A_V in the ρMC and TMC (Frerking, Langer & Wilson 1982), Whittet et al. (2001) take the threshold water ice extinction to be a marker of the transition between the diffuse outer layers of the cloud and the cold dense interior. In Fig. 4 we obtain a similar relationship between $\tau_{\text{H}_2\text{O ice}}$ and A_V for the four ρMC YSOs in our sample; the weighted fit is $0.033 \pm 0.001(A_V - 2.2 \pm 0.9)$ (dashed line). Assuming the $A_V = 6\text{--}10$ mag and $\tau_{\text{H}_2\text{O ice}}$ values for T-Elias 7S (the primary; see Section 4.8) the $\tau_{\text{H}_2\text{O ice}}$ versus A_V correlation for the TMC YSOs is probably intermediate between correlations for TMC field stars and the ρMC YSOs.

Since the change in TMC silicate properties occurs close to the ice-band threshold, we propose that the change in silicate properties

may be related to the change in the environment of the silicates. The change in the YSO silicate feature at $A_V \sim 2$ may indicate that the circumstellar dust grains surrounding low- A_V objects originated in the interface between the diffuse ISM and the outer regions of the cloud, rather than the interior of the TMC. Alternatively, the grains observed could be new grains that have recently condensed in the YSO environment. In either case, the broader features at extinctions $\gtrsim 2$ mag, which are matched better with the Trapezium emissivity are indicative of molecular cloud processing at $\lesssim 100$ K temperatures, where the dominant evolutionary processes are likely to be cosmic ray irradiation (Demyk et al. 2001) and grain coagulation.

6.4.2 Silicates in disrupted-environment YSOs

The silicates in disrupted-environment YSOs are more like those of the diffuse ISM and newly condensed dust in evolved stars than they are like TMC or Trapezium silicates. None of these YSO spectra have the 11.8- μm shoulder typical of molecular cloud dust. One interpretation of the shoulder is that it is produced by larger grains (e.g. Hanner, Brooke & Tokunaga 1994) in a dense environment such as a YSO disc or a molecular cloud. However, the shoulder is absent even in the spectrum of Elias 29, the most deeply embedded object in the sample where grain growth should be most prevalent. Since the disrupted-region YSOs are hotter and more compact than quiescent-region YSOs it is plausible that the grains have been heated sufficiently to lose all signs of low-temperature processing or have been recondensed in the circumstellar environment. Another possibility is that the dust in disrupted regions contains a much higher proportion of diffuse medium silicates than exists in quiescent regions since the star formation process may have been triggered by the shocks that shaped the molecular cloud (see Motte et al. 1998).

7 SUMMARY AND CONCLUSIONS

We have used disc and sphere models to fit UKIRT CGS3 spectra of 19 low-mass young stellar objects (YSOs) and five Herbig AeBe stars that are embedded in a variety of galactic environments including the Taurus and ρ Oph molecular clouds. Since the ρ MC was shaped by shocks associated with the expanding Scorpius H I shell and FU Ori is located on the rim of the λ Orionis CO ring, we call these objects ‘disrupted-region’ YSOs and objects in quiescent regions ‘quiescent-region’ YSOs.

χ^2_ν fitting of the 10- μm spectra does not distinguish between disc and sphere models. However, the relationship between fitted values of the disc and sphere temperature indices are close to the value in the optically thick limit, $q_s \sim 3/2q_d$.

10 out of 14 of the quiescent-region low-mass YSOs and four out of five of these Herbig AeBe stars have optically thin silicate ($\tau_{\text{emiss}} < 1.0$) emission at 10 μm . However, only one of the five disrupted-region YSOs is optically thin.

The 13 quiescent-region YSOs with non-photospheric spectra have disc temperature indices in the range 0.2–0.5 with a mean and standard deviation of $\bar{q}_d = 0.35 \pm 0.07$, the mean for the five Herbig AeBe stars is $\bar{q}_d = 0.38 \pm 0.08$. Disc temperature indices close to 0.4 indicate that the emission arises from optically thin layers above a flared optically thick disc (Chiang & Goldreich 1997). However, the temperature index could have been reduced by the effects of grain condensation and evaporation (Boss & Yorke 1996). YSOs in the ρ MC and FU Ori have a wider range of temperature indices (0.3–0.8). ρ -Elias 29 ($q_d = 0.83$) is the only source with a temperature index indicative of a flat optically thick disc $q_d \sim 0.75$. The photosphere-like continuum of Taurus-Elias 18 could be fitted

only with truncated optically thick models, implying the presence of a void between the >500 -K and cold ($\lesssim 100$ K) foreground dust and no temperature index or disc size could be inferred for this object.

The radii of the peak 10- μm emission for the majority (nine out of 13) of the quiescent-region low-mass YSOs and Herbig AeBe stars is in the 10–140 au range. However, the discs of the five disrupted-region low-mass YSOs are more compact: none of the sample is larger than 80 au and three out of five are $\lesssim 2$ au in size; this is consistent with 1.3-mm continuum observations that ρ MC YSOs are much more compact than are TMC YSOs. Hence, for these low-mass YSOs the galactic environment seems to have a stronger effect on constraining the extent of the disc than does the temperature and mass of the photosphere.

As in Paper I, the optically thin emission and foreground absorption in the profiles of low-mass YSOs from quiescent environments are similar to the silicate emission feature in molecular cloud dust in the Trapezium region of Orion. In contrast, the dust surrounding low-mass TMC YSOs with $A_V \lesssim 2$ mag and all ρ MC YSOs silicates ($A_V = 7\text{--}47$ mag) are more similar to the emission of newly condensed circumstellar silicates near the evolved star μ Cephei. The 10.8- μm shoulder typical of molecular cloud dust is absent from the spectra of disrupted-region YSOs; this structure may be absent because the dust has been heated in the circumstellar environments of these compact objects, or because the grains were not subjected to long periods of molecular cloud processing before star formation began. For the TMC YSOs, the inferred change in silicate chemistry at $A_V \sim 2$ occurs close to the visual extinction threshold at which grains in quiescent regions of the cloud become coated in H₂O ice ($A_V \sim 3$ mag) which may indicate a relationship between silicate mineralogy and the ice-band threshold.

ACKNOWLEDGMENTS

We thank M. S. Hanner and R. J. Sylvester for providing ascii files of their data. JEB, AJA and JAY are funded by PPARC. We thank Endrik Kruegel for a constructive review.

REFERENCES

- Adams F.C., Lada C.J., Shu F.H., 1988, ApJ, 326, 865
- Ageorges N., Menard F., Monin J.-L., Eckart A., 1994, A&A, 283, L5
- Aspin C., McCaughrean M.J., McLean I.S., 1985, A&A, 144, 220
- Asselin L., Ménard F., Bastien P., Monin J.-L., Rouan D., 1996, ApJ, 472, 349
- Bastien P., 1982, A&AS, 48, 153, 513
- Beckwith S.V.W., Sargent A.I., Chini R.S., Guesten R., 1990, AJ, 99, 924
- Blitz L., Williams J.P., 1997, ApJ, 488, 145
- Boss A.P., Yorke H.W., 1996, ApJ, 469, 366
- Bowey J.E., Adamson A.J., 2001, MNRAS, 320, 131 (Paper I)
- Bowey J.E., Adamson A.J., 2002, MNRAS, 334, 94
- Bowey J.E., Adamson A.J., Whittet D.C.B., 1998, MNRAS, 298, 131
- Carpenter J.M., Snell R.L., Schloerb F.P., 1995, ApJ, 445, 246
- Chiang E.I., Goldreich P., 1997, ApJ, 490, 368
- Chiar J.E., Adamson A.J., Kerr T.H., Whittet D.C.B., 1995, ApJ, 455, 234
- Chrysostomou A., Clark S.G., Hough J.H., Gledhill T.M., McCall A., Tamura M., 1996, MNRAS, 278, 449
- Cohen M., 1977, ApJ, 215, 533
- Cohen M., Bieging J.H., 1986, AJ, 92, 1396
- Cohen M., Kuhl L.V., 1979, ApJS, 41, 743
- Cohen M., Woolf N.J., 1971, ApJ, 169, 543
- Corcoran M., Ray T.P., 1998, A&A, 336, 535
- Demyk K. et al., 2001, A&A, 368, L38
- Devine D., Reipurth B., Bally J., Balonek T.J., 1999, AJ, 117, 2931
- de Geus E.J., 1992, A&A, 262, 258
- de Geus E.J., Bronfman L., Thaddeus P., 1990, A&A, 231, 137

- Duvert G., Guilloteau S., Ménard F., Simon M., Dutrey A., 2000, *A&A*, 355, 165
- Dyck H.M., Simon T., Zuckerman B., 1982, *ApJ*, 255, L103
- Feigelson E.D., Welty A.D., Imhoff C., Hall J.C., Etzel P.B., Phillips R.B., Lonsdale C.J., 1994, *ApJ*, 432, 373
- Folha D.F.M., Emerson J.P., 1999, *A&A*, 352, 517
- Forrest W.J., Gillett F.C., Stein W.A., 1975, *ApJ*, 195, 423
- Frerking M.A., Langer W.D., Wilson R.W., 1982, *ApJ*, 262, 590
- Friedemann C., Riemann H.G., Gürtler J., Tóth V., 1993, *A&A*, 277, 184
- Ghez A.M., Neugebauer G., Gorham P.W., Haniff C.A., Kulkarni S.R., Matthews K., Koresko C., Beckwith S., 1991, *AJ*, 102, 2066
- Ghez A.M., Neugebauer G., Matthews K., 1993, *AJ*, 106, 2005
- Gómez de Castro A.I., Fernández M., 1996, *MNRAS*, 283, 55
- Goodrich R.W., 1986, *ApJ*, 311, 882
- Greene T.P., Lada C.J., 2000, *AJ*, 120, 430
- Greene T.P., Meyer M.R., 1995, *ApJ*, 450, 233
- Greene T.P., Wilking B.A., Andre P., Young E.T., Lada C.J., 1994, *ApJ*, 434, 614
- Grinin V.P., Kiselev N.N., Minikulov N. Kh., Chernova G.P., 1988, *Sov. Astron. Lett.*, 14, 219
- Grinin V.P., Kozlova O.V., Thé P.S., Rostopchina A.N., 1996, *A&A*, 309, 474
- Hamann F., Persson S.E., 1992, *ApJ*, 394, 628
- Hanner M.S., Brooke T.Y., Tokunaga A.T., 1994, *ApJ*, 433, L97
- Hanner M.S., Brooke T.Y., Tokunaga A.T., 1995, *ApJ*, 438, 250 (HBT1995)
- Hanner M.S., Brooke T.Y., Tokunaga A.T., 1998, *ApJ*, 502, 871 (HBT1998)
- Hartigan P., Kenyon S.J., Hartmann L., Strom S.E., Edwards S., Welty A.D., Stauffer J., 1991, *ApJ*, 382, 617
- Herbig G.H., 1960, *ApJS*, 4, 337
- Herbig G.H., 1966, *Vistas Astron.*, 8, 109
- Herbig G.H., 1977, *ApJ*, 217, 693
- Hessman F.V., Guenther E.W., 1997, *A&A*, 321, 497
- Hillenbrand L.A., Strom S.E., Vrba F.J., Keene J., 1992, *ApJ*, 397, 613
- Hojaev A.S., 1999, *New Astron. Rev.*, 43, 431
- Kenyon S.J., Hartmann L.W., Kolotilov E.A., 1991, *PASP*, 103, 1069
- Kenyon S.J., Hartmann L., 1995, *ApJS*, 101, 117
- Kenyon S.J., Kolotilov E.A., Ibragimov M.A., Mattei J.A., 2000, *ApJ*, 531, 1028
- Kerr T.H., Adamson A.J., Whittet D.C.B., 1993, *MNRAS*, 262, 1047
- Kobayashi N., Nagata T., Tamura M., Takeuchi T., Takami H., Sato S., 1997, *ApJ*, 481, 936
- Kolotilov E.A., Kenyon S.J., 1997, *Inf. Bull. Variable Stars*, 4494
- Kolotilov E.A., Zaitseva G.V., Shenavrin V.I., 1977, *Astrofizika*, 13, 449
- Lagage P.O., Olofsson G., Cabrit S., Cesarsky C.J., Nordh L., Rodriguez Espinosa J.M., 1993, *ApJ*, L79
- Lang W.J., Masheder M.R.W., Dame T.M., Thaddeus P., 2000, *A&A*, 357, 1001
- Leinert C., Richichi A., Haas M., 1997, *A&A*, 318, 472
- Leinert C., Beck T.L., Ligi S., Simon M., Woitas J., Howell R.R., 2001, *A&A*, 369, 215
- Leinert C., Haas M., Weitzel N., 1993, *A&A*, 271, 535
- Li W., Evans N.J., Harvey P.M., Colomé C., 1994, *ApJ*, 433, 199
- Luhman K.L., Rieke G.H., 1999, *ApJ*, 525, 440
- McMuldrough S., Sargent A.I., Blake G.A., 1993, *AJ*, 106, 2477
- Malbet F. et al., 1998, *ApJ*, 507, L149
- Mannings V., Sargent A.I., 1997, *ApJ*, 490, 792
- Martin P.G., Whittet D.C.B., 1990, *ApJ*, 357, 113
- Meeus G., Waters L.B.F.M., Bouwman J., van den Ancker M.E., Waelkens C., Malfait K., 2001, *A&A*, 365, 476
- Ménard F., Monin J., Angelucci F., Rouan D., 1993, *ApJ*, 414, L117
- Millan-Gabet R., Schloerb F.P., Traub W.A., 2001, *ApJ*, 546, 358
- Minchin N.R., Hough J.R., Burton M.G., Yamashita T., 1991, *MNRAS*, 251, 522
- Monin J.L., Ménard F., Duchêne G., 1998, *A&A*, 339, 113
- Motte F., Andre P., Neri R., 1998, *A&A*, 336, 150
- Movsessian T.A., Magakian T.Y., 1999, *A&A*, 347, 266
- Mundt R., Eisloffel J., 1998, *AJ*, 116, 860
- Murakawa K., Tamura M., Nagata T., 2000, *ApJS*, 128, 603
- Nakajima T., Golimowski D.A., 1995, *AJ*, 109, 1181
- Natta A., Palla F., Butner H.M., Eveans N.J., Harvey P.M., 1993, *ApJ*, 406, 674
- Natta A., Meyer M.R., Beckwith S.V.W., 2000, *ApJ*, 534, 838
- Petrov P.P., Gullbring E., Ilyin I., Gahm G.F., Tuominen I., Hackman T., Loden K., 1996, *A&A*, 314, 821
- Petrov P., Duemmler R., Ilyin I., Tuominen I., 1998, 331, *A&A*, L53
- Phillips R.B., Lonsdale C.J., Feigelson E.D., 1991, *ApJ*, 382, 261
- Reipurth B., Zinnecker H., 1993, *A&A*, 278, 81
- Richichi A., Leinert C., Jameson R., Zinnecker H., 1994, *A&A*, 287, 145
- Russell R.W., Soifer B.T., Forrest W.J., 1975, *ApJ*, 198, L41
- Shevchenko V.S., Yakubov S.D., Hambarian V.V., Garibjanian A.T., 1991, *AZh*, 68, 275
- Shirt J.V., Warren-Smith R.F., Scarrott S.M., 1983, *MNRAS*, 204, 1257
- Shuping R.Y., Chiar J.E., Snow T.P., Kerr T., 2001, *ApJ*, 547, L161
- Simon T., Joyce R.R., 1988, *PASP*, 100, 1549
- Simon T., Morrison N.D., Wolff S.C., Morrison D., 1972, *A&A*, 20, 99
- Skinner S.L., Walter F.M., 1998, *ApJ*, 509, 761
- Smith C.H., Wright C.M., Aitken D.K., Roche P.F., Hough J.H., 2000, *MNRAS*, 312, 327
- Smith R.G., Sellgren K., Tokunaga A.T., 1989, *ApJ*, 344, 413
- Smith R.G., Sellgren K., Brooke K.Y., 1993, *MNRAS*, 263, 749
- Strom K.M., Kepner J., Strom S.E., 1995, *ApJ*, 438, 813
- Sylvester R.J., Mannings V., 2000, *MNRAS*, 313, 73
- Tanaka M., Sato S., Nagata T., Yamamoto T., 1990, *ApJ*, 352, 724
- Teixeira T.C., Emerson J.P., 1999, *A&A*, 351, 303
- Teixeira T.C., Emerson J.P., Palumbo M.E., 1998, *A&A*, 330, 711
- Terranegra L., Chavarria-K. C., Diaz S., Gonzalez-Patino D., 1994, *A&AS*, 104, 557
- Tsuboi Y., Koyama K., Murakami H., Hayashi M., Skinner S., Ueno S., 1998, *ApJ*, 503, 894
- Tsuboi Y., Imanishi K., Koyama K., Grosso N., Montmerle T., 2000, *ApJ*, 532, 1089
- Ungerechts H., Thaddeus P., 1987, *ApJS*, 63, 645
- Van Cleve J.E., Hayward T.L., Miles J.W., Gull G.E., Shoenwald J., Houck J.R., 1994, *Ap&SS*, 212, 231
- van den Ancker M.E., de Winter D., Tjin A Djie H.R.E., 1998, *A&A*, 330, 145
- Weintraub D.A., Kastner J.H., Griffith Laura L., Campins H., 1993, *AJ*, 105, 271
- Welty A.D., 1995, *AJ*, 110, 776
- Whittet D.C.B., 1992, *Dust in the galactic environment*. IOP Publishing Ltd, Bristol
- Whittet D.C.B., Bode M.F., Longmore A.J., Adamson A.J., McFadzean A.D., Aitken D.K., Roche P.F., 1988, *MNRAS*, 233, 321
- Whittet D.C.B., Gerakines P.A., Hough J.H., Shenoy S.S., 2001, *ApJ*, 547, 872
- Zhang Q., Wootten A., Ho P.T.P., 1997, *ApJ*, 475, 713

APPENDIX A: QUIESCENT-REGION YSOs

A1 Taurus molecular cloud sources

A1.1 *T-Elias 7 (Har06-10, GV Tau)*

The nature of Elias 7 was discussed in detail in Paper I. More recent optical imaging reveals a Herbig–Haro outflow emanating from the northern component (Movsessian & Magakian 1999), whilst $H\alpha$ images (Devine et al. 1999) show more complex structures that may result from increased mass ejection at periastron. This system shows significant variability in near-infrared images (Leinert et al. 2001). Since only the southern component suffers silicate absorption, the northern component was subtracted before fitting the silicate feature (see Paper I).

A1.2 T Tauri

T Tauri is a binary separated by 0.7 arcsec in a N–S direction (Dyck, Simon & Zuckerman 1982); a northern classical T Tauri star, with a southern infrared companion that suffered a 2 mag near- to mid-infrared FU Ori outburst between 1989 and 1991 (Ghez et al. 1991). During this period Kobayashi et al. (1997) observed two distinct polarization components between 0.9 and 2.5 μm : shortwards of 1.6 μm the polarization is consistent with the local interstellar extinction towards T Tauri North; longwards of 1.6 μm the polarization angle of 20° and is associated with T Tauri South because the percentage polarization increased during the outburst of this object. In 10.1- μm long-slit scans the flux distribution was dominated by T Tauri N in 1985, and by T Tauri South in 1990 (Ghez et al. 1991); between 1990 October and 1991 January their infrared spectral energy distribution (SED) suggested a 10- μm silicate emission feature towards the primary and an absorption feature towards the IRC; the 10.1- μm flux of the primary was constant during this period. Mid-infrared images of the system obtained by van Cleve et al. (1994) in 1992 November indicate a silicate absorption feature for the system, silicate absorption towards the IRC and a weaker emission feature towards T Tauri N, there is insufficient spectral resolution to determine whether the emission is optically thin or thick. We model the northern component of the flux spectrum of the binary obtained by HBT1998 in 1993 November after subtracting the flux of T Tauri N. This was estimated by extrapolating the Van Cleve et al. flux ratios of the N and S components to 13.5 μm and interpolating them to our wavelength scale (see Fig. A1). We therefore assume that the ratios did not change between 1992 November and 1993 November; for reference we show the fluxes obtained by Ghez et al. in 1991 January.

A1.3 Haro 6-13

Teixeira & Emerson (1999) estimate an $A_V \sim 9.5$ and list the source as a continuum source. We used a temperature of 4000 K to model the source.

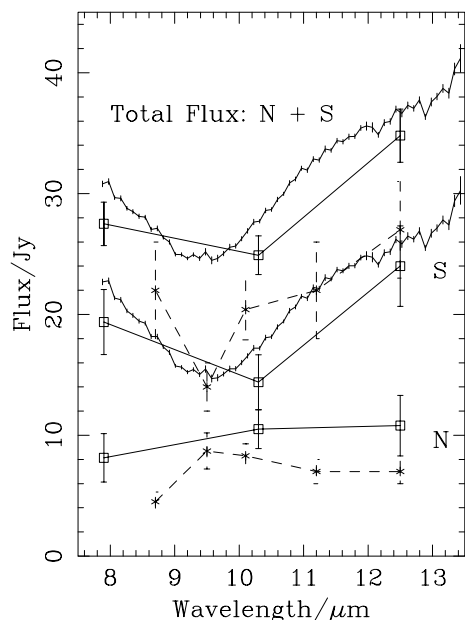


Figure A1. Separating the fluxes owing to the binary components of T Tauri; photometry solid lines: Van Cleve et al. 1994; dashed lines: Ghez et al. (1991). The estimated spectrum of the southern component was obtained by subtracting Van Cleve et al.'s fluxes for the northern (optical) star.

A1.4 HP Tau

HP Tau is in a complicated system consisting of HP Tau, HP Tau G2 and HP Tau G3, HP Tau and HP Tau G3 are surrounded by an arc-like reflection nebula 30 arcsec in radius. Since HP Tau is 20.9 arcsec from G2 and 9.7 arcsec from G3 (Monin, Ménard & Duchêne 1998), we assume that only HP Tau itself was observed in the 5.5-arcsec slit of CGS 3. In the submillimetre band, continuum emission is observed only from HP Tau (Duvert et al. 2000); variable radio emission is observed only from G3 and G2 (Cohen & Bieging 1986). HP Tau and HP Tau/G3 are both binaries with binary separations of 0.02 arcsec (Richichi et al. 1994). We used a spectral type of K3 and $A_V = 2.26$ (Kenyon & Hartmann 1995).

A1.5 SU Aur

SU Aur has the highest X-ray luminosity of any classical T Tauri star; this emission varies on a time-scale of a few days (e.g. Skinner & Walter 1998). *UBV* photometry reveals the simultaneous occurrence of mass infall and outflow in the line of sight to the star (e.g. Petrov et al. 1996). This indicates an impulsive outflow of gas in the circumstellar envelope that may produce expanding shells and which decelerates beyond 3 stellar radii. Magnetic accretion modelling of the simultaneous inflow in the innermost region suggests that the object is seen almost edge-on (Petrov et al. 1996). Following Beckwith et al. (1990) we used a spectral type of G2III and $A_V = 1.45$.

A1.6 V773 Tau (HD 283447)

V773 Tau is a magnetically active X-ray and radio bright (e.g. Feigelson et al. 1994) system that has no visible reflection nebula (Nakajima & Golimowski 1995). In 1995 the source exhibited an X-ray flare lasting several hours, which reached a temperature $> 10^8$ K (Tsuboi et al. 1998). Ghez, Neugebauer & Matthews (1993) found a companion at a separation of 112 mas by IR speckle imaging. Welty (1995) discovered that the source is really a spectroscopic binary with a period of 51.075 d and an orbit diameter of 2.5 mas. The object is surrounded by a source of variable radio emission that evolved from an ultracompact to an extended source of 24–34 stellar radii (2.5 mas) which is comparable to the diameter of the binary orbit (Phillips, Lonsdale & Feigelson 1991). The source was modelled with a spectral type of K3 and $A_V = 1.32$ (Kenyon & Hartmann 1995).

A1.7 DK Tau (Elias 8)

DK Tau is a binary separated by 2.5 arcsec; the primary has a spectral type of K9 and that of the secondary is M1 (Monin et al. 1998), $A_V = 1.3$ (Hartigan et al. 1991).

A2 Other quiescent-region YSOs

A2.1 V1057 Cyg (LkH α 190)

V1057 Cyg lies in a dense dust pocket in the H II region NGC 7000. The object was thought to be a normal T Tauri star until 1970 when its visual magnitude increased by 5.5 mag in 390 d as high-velocity shells were ejected (Herbig 1977); therefore it is now classified as an FU Ori star. 0.7 yr after maximum its classification was A3-5II in blue, F5 in red, though by 1976 its red spectral type was G2-5Ib-II in the red. 2.2–22 μm photometry in 1971 March suggested a reddened

stellar continuum plus a very cool circumstellar silicate shell (Cohen & Woolf 1971). By 1995 the object went into a minimum brightness before reaching its pre-outburst flux in the *B* band (Petrov et al. 1998). The flare in brightness is associated with the eruption of a cool expanding shell of gas and the subsequent dimming with dust condensation (Kolotilov & Kenyon 1997). Herbig suggested that if there was a circumstellar disc that the object is viewed pole on. Given the flux variation and change in veiling over the intervening years the true spectral type of this source and visual extinction at the time of the observations by HBT1998 is extremely uncertain. Therefore, we adopt a spectral type of K1V and use $A_V = 3.6$ (Simon et al. 1988).

A2.2 V536 Aql

V536 Aql has a large 6–8 per cent optical linear polarization, implying the presence of asymmetrically distributed material around the star (Bastien 1982). *J*-, *H*- and *K*-band images show that the source is a binary with a projected separation of 0.52 arcsec at PA $\sim 17^\circ$ (Ageorges et al. 1994). The spectral type of the system is a K7 T Tauri with $A_V = 3.6$ mag (Cohen & Kuhl 1979). Optical images of V536 Aql show a deflected jet of blueshifted S II emission knots at PA $\simeq 110^\circ$ between 4.2 and 16 arcsec from the star (Mundt & Eislöffel 1998).

A2.3 V1515 Cyg

V1515 Cyg is an optically faint FU Ori star with a ring-shaped reflection nebula that took 25 yr to reach its maximum before experiencing a dramatic optical brightness decline in 1980 that has been associated with a dust forming event. The A_V is 2.8 ± 0.3 mag (Kenyon, Hartmann & Kolotilov 1991). The estimated spectral type is K2 (Terranegra et al. 1994).

A2.4 V1331 Cyg (*LkH α 120*)

V1331 Cyg is located in the dark cloud Lynds 984. It is an FU Ori pre-outburst candidate. Estimations of spectral class range from G and F0–2 to B0.5 with $A_V = 2.4$ mag. In the *R* band its angular size is 47×53 arcsec² with a fountain-like shape (Hojaev 1999). Shevchenko et al. (1991) estimated a distance of 550 pc. Optical continuum and S II emission images reveal a strongly wiggling jet to the south and emission knots to the north that correspond to a 1-pc bipolar jet (Mundt & Eislöffel 1998). They estimate that the angle of the poles to the line of sight is 42° . Radio observations of CO molecular emission reveal that the northern jet is blueshifted, the southern redshifted and a gaseous ring 4.1×10^4 by 2.8×10^4 au in size with a maximum velocity dispersion of 20 km s⁻¹ and an inclination of $\sim 40^\circ$ (McMuldrough, Sargent & Blake 1993).

A2.5 DI Cep

DI Cep has a UV hotspot covering 1–3 per cent of its photosphere owing to magnetically channelled accretion of material from a disc on to the stellar surface (Gómez de Castro & Fernández 1996). Variability in the redshifted wings of the H α and H β emission lines also indicates the presence of infalling matter (Hessman & Guenther 1997). Veiling is negligible in the *V*–*J* bands (Gómez de Castro & Fernández 1996), but is high in the *K* band (Folha & Emerson 1999). Optical data indicate a spectral type of G8IV (Hessman & Guenther 1997) and $A_V = 0.9$ mag (Hamann & Persson 1992).

APPENDIX B: DISRUPTED-REGION YSOs

B1 ρ Ophiuchi molecular cloud sources

B1.1 Elias 29 (*WL 15*)

Elias 29 is a class I low-mass protostar with deep water ice and substantial CO ice absorption features – $\tau = 1.8$ (Tanaka et al. 1990) and 0.35 (Kerr, Adamson & Whittet 1993), respectively, and $A_V \sim 47$ mag. Three periodic X-ray flares were detected in 20 h (Tsuboi et al. 2000). Its high visual extinction is consistent with the high near-infrared veiling observed by Greene & Lada (2000). Spectropolarimetry of this source suggests that the 10- μ m emission in this source is optically thick (Smith et al. 2000).

B1.2 Elias 21 (*GSS 30*)

Elias 21 is associated with a bi-polar reflection nebula inclined towards the observer by 25° (Weintraub et al. 1993; Chrysostomou et al. 1996) so that the northern lobe is in front of a disc that obscures the southern lobe. Up to four sources (IRS1–4) can be observed in NIR images. IRS1 illuminates the nebula, but IRS2 is not physically associated with it, IRS 3 and 4 appear only in *K*-band images (Weintraub et al.). The nebula illuminates a CO core that is orthogonal to the nebula and 30×20 arcsec² in extent (Zhang, Wootten & Ho 1997). Tanaka et al. (1990) observe a strong 3.1- μ m ice absorption, which may come from an edge-on disc. We adopt a spectral type of M2, giving an effective temperature of 3400 K and A_V of 22.6 mag (for GSS 30 IRS 2; Greene & Meyer 1995).

B1.3 Elias 23 (*GY 23, S2, GSS 32*)

S2 is a binary separated by 10.6 arcsec. Since the *K*-band primary is 3.1 mag brighter than the secondary, we assume that only the brighter source was observed at 10 μ m. Near-IR photometry suggests a disc plus optically thin emission (Strom, Kepner & Strom 1995). The presence of water ice (Tanaka et al. 1990) but little CO ice ($\tau_{4.67\mu\text{m}} < 0.10$; Kerr et al. 1993) imply that the disc is inclined to the line of sight since CO is more volatile than H₂O. The spectral type of the source is K5–M2 and $A_J = 3.1$ (Luhman & Rieke 1999) giving a visual extinction of 10.2 mag. We modelled the source as a K7V with an effective temperature of 4000 K.

B1.4 Elias 28 (*SR 24 N and S, GY168 and GY 167*)

Elias 28 is a binary separated by 7 arcsec in declination. We do not know which component was observed by HBT1995. Since the southern component is brighter than the northern component in the infrared and 0.6 mag brighter in the *N* band (Greene et al. 1994) we model the 10- μ m spectrum with parameters derived for this source. Luhmann & Rieke (1999) estimate that Elias 28S is of spectral type G5–K7 and $A_J = 1.2$ giving $A_V = 3.9$. (Elias 28N is of spectral type K5–M2 with $A_J = 2.0$, giving $A_V = 6.6$). The NIR extinctions for the binary components are lower than values derived from the SED by Greene et al. who obtain A_V values of 10.6 and 10.4, respectively, for the northern and southern components.

B2 FU Ori

Aperiodic $\lesssim 1$ d 0.035-mag fluctuations in the *UBV* bands indicates accretion is occurring at the inner edge of a disc (Kenyon et al. 2000). The source has been resolved to 2 au in the *K* band (Malbet

et al. 1998). Kenyon et al. (2000) estimate a spectral type of G0II (so $T_* \sim 5500$ K) and $A_V = 2.2$.

APPENDIX C: HERBIG AeBe STARS

C0.1 V645 Cyg

Kinematically, the nebula lies in the Cassiopeia–Perseus spiral arm, at a distance of 3.5 kpc; the spectral type is A0I and $A_V = 2.6$ mag (Goodrich 1986). V645 Cyg (GL 2789) consists of two luminous knots, N0 and N1 (Cohen 1977). N0 is compact and N1 is elongated in the north-east to south-west direction. J -, H - and K -band imaging polarimetry (Minchin et al. 1991) indicates an edge-on disc of $\sim 8 \times 10^4 \times 4 \times 10^4$ au centred on N0. N1 is produced by scattering on a dense slab of material that has been swept up from the disc by the outflow. The 10- μm polarization spectrum of this object peaks at ~ 10.2 μm , which indicates the feature is due entirely to silicate absorption (Smith et al. 2000). The imaged FWHM is $\lesssim 14$ arcsec at 50 μm and 22 ± 2 at 100 μm (Natta et al. 1993).

C0.2 LkH α 233

LkH α 233 is located in condensation A of the Lac OB1 molecular cloud. V -, J - and H -band images reveal a rectangular nebula (Aspin, McCaughrean & McLean 1985; Li et al. 1994), implying the presence of a circumstellar disc or torus of aligned grains and bipolar lobes. Corcoran & Ray (1998) inferred a $\lesssim 600$ au radius disc from the occultation of the redshifted lobe in S II images; close to the star they resolved two velocity components, which indicate the presence of a low-velocity disc wind, in addition to the high-velocity Herbig–Haro jet. K -band speckle interferometry indicates the source is embedded in a symmetrical scattering halo with a FWHM of 1.2 ± 0.2 arcsec (~ 1000 au; Leinert, Haas & Weitzel 1993). We adopt $A_V \sim 2.6$ (Aspin et al. 1985) and a spectral type of A7 is from (Herbig 1960).

C0.3 LkH α 208

LkH α 208 is associated with an optical bipolar reflection nebula (Shirt, Warren-Smith & Scarrott 1983); imaging polarimetry reveals that the source is slightly extended along the minor axis of the nebula and parallel to a dust ring of mass $0.3 M_\odot$. There is little or no tilt of the major axis of the nebula with respect to the line of

sight. The southern lobe of the nebula suffers extinction by a ring or disc. LkH α 208 is a binary Ae/Be star with a projected separation of 0.115 (115 au) with a brightness ratio at K or 0.54 (Leinert, Richichi & Haas 1997). LkH α 208 is in front of the Gem OB1 molecular cloud complex (Carpenter, Snell & Schloerb 1995). The spectral type of B7 and $A_V \sim 1.7$ were deduced by Hillenbrand et al. (1992).

C0.4 HD 150193; Elias 2-49; MWC 863

HD 150193 is a visual and spectroscopic binary Herbig AeBe star with a separation of 1.1 arcsec or 176 au (Reipurth & Zinnecker 1993); the PA of the secondary is 227° . Since the primary is 2.3 and 3.1 mag brighter, respectively, in the K and L' bands, we adopt a spectral type of A2 (that of the secondary is K4; Millan-Gabay, Schloerb & Traub 2001). The visual extinction towards the primary is 1.61 (van den Ancker, de Winter & Tjin A Djie 1998). HD 150193 has also been listed as a Vega-like star. However, Sylvester & Mannings (2000) found that the flux of the 10- μm spectrum is 65 times larger than it would be if dominated by photospheric emission and concluded that this is owing to accretion in a YSO disc, rather than from a remnant disc.

C0.5 WW Vul

Optical polarimetry indicates that the symmetry axis of the circumstellar disc may be oriented parallel to the local interstellar magnetic field (Grinin et al. 1988). WW Vul displays aperiodic variation in the V – R bands, which may be consistent with a clumpy and dusty circumstellar envelope with $A_V \sim 0.64$ mag (Friedemann et al. 1993). There is no correlation between changes in the UBV and J - to L -band variability (Kolotilov, Zaitseva & Shenavrin 1977). There is no evidence of extended emission in the H and J bands (Li et al. 1994). Wavelength shifts in the Na I D lines indicate the occasional infall of matter on to the star with maximum radial velocities of 250 km s^{-1} whilst low-velocity components ($\geq 30 \text{ km s}^{-1}$) indicate gas motions to and from the star. The H α line profile is indicative of a 400 km s^{-1} rotating gas. These indicate (respectively) the infall of star-grazing comets and gas accretion of remnants of the protostellar cloud (Grinin et al. 1996).

This paper has been typeset from a $\text{\TeX}/\text{\LaTeX}$ file prepared by the author.